

Contrastive Attraction and Contrastive Repulsion for Representation Learning

Huangjie Zheng^{*1} Xu Chen^{* 234} Jiangchao Yao⁴ Hongxia Yang⁴ Chunyuan Li⁵
 Ya Zhang² Hao Zhang⁶ Ivor W. Tsang³ Jingren Zhou⁴ Mingyuan Zhou¹
¹The University of Texas at Austin ²Shanghai Jiao Tong University
³University of Technology Sydney ⁴Alibaba Group ⁵Microsoft Research ⁶Cornell University

Abstract

Contrastive learning (CL) is effective in learning data representations without label supervision, where the encoder needs to contrast each positive sample over multiple negative samples via a one-vs-many softmax cross-entropy loss. However, conventional CL is sensitive to how many negative samples are included and how they are selected. Proposed in this paper is a doubly CL strategy that contrasts positive samples and negative ones within themselves separately. We realize this strategy with contrastive attraction and contrastive repulsion (CACR) makes the query not only exert a greater force to attract more distant positive samples but also do so to repel closer negative samples. Theoretical analysis reveals the connection between CACR and CL from the perspectives of both positive attraction and negative repulsion and shows the benefits in both efficiency and robustness brought by separately contrasting within the sampled positive and negative pairs. Extensive large-scale experiments on standard vision tasks show that CACR not only consistently outperforms existing CL methods on benchmark datasets in representation learning, but also provides interpretable contrastive weights, demonstrating the efficacy of the proposed doubly contrastive strategy.

1 Introduction

The conventional Contrastive Learning (CL) loss (Oord et al., 2018; Poole et al., 2018) has achieved remarkable success in representation learning, benefiting downstream tasks in a variety of areas (Misra and Maaten, 2020; He et al., 2020; Chen et al., 2020a; Fang and Xie, 2020; Giorgi et al., 2020). Recent approaches mainly apply the conventional CL loss to make the encoder distinguish each positive sample within multiple negative samples. In image representation learning, this scheme is widely used to encourage the encoder to learn representations that are invariant to unnecessary details in the representation space, for which the unit hypersphere is the most common assumption (Wang et al., 2017; Davidson et al., 2018; Hjelm et al., 2018; Tian et al., 2019; Bachman et al., 2019). Meanwhile, the contrast with negative samples is demystified as avoiding the collapse issue, where the encoder outputs a trivial constant, and uniformly distributing samples on the hypersphere (Wang and Isola, 2020). To improve the quality of the contrast, various methods, such as large negative memory bank (Chen et al., 2020b), hard negative mining (Chuang et al., 2020; Kalantidis et al., 2020), and using strong or multi-view augmentations (Chen et al., 2020a; Tian et al., 2019), are proposed and succeed in learning powerful representations. Since the conventional CL loss achieves the one-vs-many contrast with a softmax cross-entropy loss, a notable concern is still that the contrast could be sensitive to the sampled positive and negative pairs (Saunshi et al., 2019; Chuang et al., 2020). Given a sampled query, a conventional CL method usually randomly takes one positive sample, and equally treats all the other negative samples, regardless of how informative they are to the query. The sampled positive pair could make the contrast either easy or difficult, and trivially selecting hard negative pairs could make the optimization inflexible and inefficient.

An alternative intuition of the CL loss is that given a query, its positive sample needs to be close, while its negative ones need to be far away in the representation space. This motivates the construction of Contrastive Attraction and Contrastive Repulsion (CACR), a new CL framework where the positive and negative samples are first contrasted within themselves before getting pulled and pushed, respectively, from the query. As shown in Figure 1, unlike conventional CL, which equally treats samples and pulls/pushes them with the softmax cross-entropy contrast, CACR considers both

^{*}Equal contribution

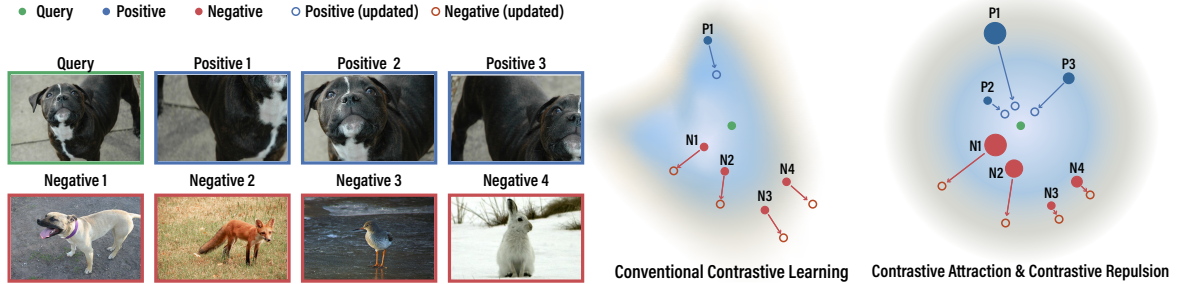


Figure 1: Comparison of conventional contrastive learning (CL) and the proposed Contrastive Attraction and Contrastive Repulsion (CACR) framework. For conventional CL, given a query, the model randomly takes one positive sample to form a positive pair and compares it against multiple negative pairs, with all samples equally treated. For CACR, using multiple positive and negative pairs, the weight of a sample (indicated by point scale) is contrastively computed to allow the query to not only more strongly pull more distant positive samples, but also more strongly push away closer negative samples.

the cost of moving positive samples close and that of moving negative samples away. Moreover, CACR applies a double-contrast strategy to contrast the positive samples and negative ones within themselves separately, where we formulate the contrasts as the conditional probabilities of moving a given query to different samples. Specifically, if a selected positive sample is far away from the query, it indicates the encoder does not sufficiently capture some information, and CACR will assign higher probability for the query to pull this positive sample. Conversely, if a selected negative sample is too close to the query, it indicates the encoder has difficulty distinguishing them, and CACR will assign higher probability for the query to push away this negative sample. This double-contrast method determines if a positive/negative sample is easy or hard to move, making the optimization more flexible.

We further provide theoretical analysis of CACR’s properties to show the connection and difference between CACR and conventional CL methods. We also justify the effectiveness of the doubly contrastive strategy from both theoretical and empirical perspectives. Our main contributions include: 1) We propose CACR, a CL framework where the positive and negative samples first contrast within themselves respectively, with the importance of positive and negative samples modeled by two separate conditional distributions. With the weight of a sample indicating how informative it is to the query, CACR is able to attract positive samples close and repel negative samples away from the query in a more efficient and adaptive way. 2) CACR produces useful representations by minimizing the expected cost of attracting the positive samples towards the query while maximizing that of pushing the negative samples away from the query. The doubly contrastive strategy is realized by modeling two conditional distributions for the intra-contrasts within positive and negative samples. Our theoretical and empirical analysis show that these two conditional distributions help in making contrastive attraction and contrastive repulsion more effective and robust than conventional CL does. 3) Our experiments show that CACR consistently outperforms conventional CL methods in a variety of settings, achieving state-of-the-art results on standard vision tasks over various benchmark datasets.

2 Related work

Plenty of unsupervised representation learning (Bengio et al., 2013) methods have been developed to learn good data representations, *e.g.*, PCA (Tipping and Bishop, 1999), RBM (Hinton and Salakhutdinov, 2006), VAE (Kingma and Welling, 2014). Among them, CL (Oord et al., 2018) is investigated as a lower bound of mutual information in early stage (Gutmann and Hyvärinen, 2010; Hjelm et al., 2018). Recently, many studies reveal that the effectiveness of CL is not just attributed to the maximization of mutual information (Tschannen et al., 2019; Tian et al., 2020a), motivating various works to demystify the contrastive learning scheme.

Contrastive representation learning. In vision tasks, SimCLR (Chen et al., 2020a;c) studies extensive augmentations for positive and negative samples and intra-batch-based negative sampling. A memory bank that caches representations (Wu et al., 2018) and a momentum update strategy are introduced to enable the use of an enormous number of negative samples (He et al., 2020; Chen et al., 2020b). CL has also been developed in learning representations for text (Logeswaran and Lee, 2018), sequential data (Oord et al., 2018; Hénaff et al., 2019), structural data like graphs (Sun et al., 2020; Li et al., 2019; Hassani and Khasahmadi, 2020; Velickovic et al., 2019), reinforcement learning (Srinivas et al., 2020), and few-shot scenarios (Khosla et al., 2020; Sylvain et al., 2020). Along with the success of these designs, works like Wang and Isola (2020) reveal the contrastive scheme is optimizing the alignment of positive samples and the uniformity of negative pairs in the limit of an infinite number

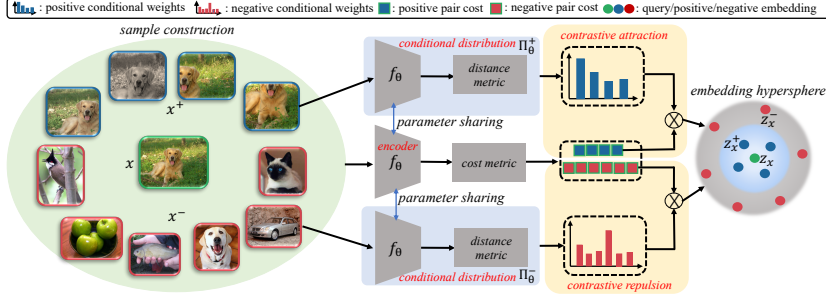


Figure 2: Illustration of the CACR framework. The encoder extracts features from samples and the conditional distributions help weigh the samples differently given the query, according to the distance of a query x and its contrastive samples x^+ , x^- . \otimes means element-wise multiplication between costs and conditional weights.

of negative samples.

Sample selection for CL. How to construct samples in CL has also been widely studied. For positive samples, Chen et al. (2020a;b) propose to apply image perturbations. Tian et al. (2019; 2020b) consider the image views in different modalities and minimize the irrelevant mutual information between them. Most works on negative selection observe the merits of using “hard” negative samples, motivating the introduction of additional techniques, such as Mixup and adversarial noise (Bose et al., 2018; Cherian and Aeron, 2020; Li et al., 2020). In a view that not all negative pairs are “true” negatives (Saunshi et al., 2019), Chuang et al. (2020) propose a decomposition of the data distribution to approximate the true negative distribution. RingCL (Wu et al., 2021) proposes to use “neither too hard nor too easy” negative samples by predefined percentiles, and HN-CL (Robinson et al., 2021) applies Monte-Carlo sampling for selecting hard negative samples. The conditional distributions in CACR also show the spirit of the sampling weights, but the objective is not limited to contrast positives and negatives in a one-vs-many mechanism as RingCL and HN-CL do. An advantage of CACR is its flexibility of the learnable conditional distributions, rather than heuristically defined based on prior belief. Compared to HN-CL (Robinson et al., 2021) inspired by the philosophy of hard negative mining, CACR is motivated by contrastively pull positives and contrastively push negatives according to how informative they are to the query. This yields two distinct loss functions shown in Section 3.1, and we further empirically explore the difference between sample selection based CL and CACR by experiments in Section 5.

3 The proposed approach

In CL, for observations $x_{0:M} \sim p_{\text{data}}(x)$, we commonly assume that each x_i can be transformed in certain ways, with the samples transformed from the same and different data regarded as positive and negative samples, respectively. Specifically, we denote $\mathcal{T}(x_i, \epsilon_i)$ as a random transformation of x_i , where $\epsilon_i \sim p(\epsilon)$ represents the randomness injected into the transformation. In computer vision, ϵ_i often represents a composition of random cropping, color jitter, Gaussian blurring, etc. For each x_0 , with query $x = \mathcal{T}(x_0, \epsilon_0)$, we sample a positive pair (x, x^+) , where $x^+ = \mathcal{T}(x_0, \epsilon^+)$, and M negative pairs $\{(x, x_i^-)\}_{1:M}$, where $x_i^- = \mathcal{T}(x_i, \epsilon_i^-)$. Denote $\tau \in \mathbb{R}^+$, where $\mathbb{R}^+ := \{x : x > 0\}$, as a temperature parameter. With encoder $f_\theta : \mathbb{R}^n \rightarrow \mathcal{S}^{d-1}$, where we follow the convention to restrict the learned d -dimensional features with a unit norm, we desire to have similar and distinct representations for positive and negative pairs, respectively, via the contrastive loss as

$$\mathbb{E}_{(x, x^+, x_{1:M}^-)} \left[-\ln \frac{e^{f_\theta(x)^\top f_\theta(x^+)/\tau}}{e^{f_\theta(x)^\top f_\theta(x^+)/\tau} + \sum_i e^{f_\theta(x)^\top f_\theta(x_i^-)/\tau}} \right]. \quad (1)$$

Note by construction, the positive sample x^+ is independent of x given x_0 and the negative samples x_i^- are independent of x . Intuitively, this 1-vs- M softmax cross-entropy encourages the encoder to not only pull the representation of a randomly selected positive sample closer to that of the query, but also push the representations of M randomly selected negative samples away from that of the query.

3.1 Contrastive attraction and contrastive repulsion

In the same spirit of letting the query attract positive samples and repel negative samples, Contrastive Attraction and Contrastive Repulsion (CACR) directly models the cost of moving from the query to positive/negative samples with a doubly contrastive strategy:

$$\begin{aligned}\mathcal{L}_{\text{CACR}} &:= \underbrace{\mathbb{E}_{\mathbf{x} \sim p(\mathbf{x})} \mathbb{E}_{\mathbf{x}^+ \sim \pi_{\theta}^+(\cdot | \mathbf{x}, \mathbf{x}_0)} [c(f_{\theta}(\mathbf{x}), f_{\theta}(\mathbf{x}^+))]}_{\text{Contrastive Attraction}} + \underbrace{\mathbb{E}_{\mathbf{x} \sim p(\mathbf{x})} \mathbb{E}_{\mathbf{x}^- \sim \pi_{\theta}^-(\cdot | \mathbf{x})} [-c(f_{\theta}(\mathbf{x}), f_{\theta}(\mathbf{x}^-))]}_{\text{Contrastive Repulsion}}, \\ &:= \mathcal{L}_{\text{CA}} + \mathcal{L}_{\text{CR}},\end{aligned}\tag{2}$$

where we denote π^+ and π^- as the conditional distributions of intra-positive contrasts and intra-negative contrasts, respectively, and $c(\mathbf{z}_1, \mathbf{z}_2)$ as the point-to-point cost of moving between two vectors \mathbf{z}_1 and \mathbf{z}_2 , *e.g.*, the squared Euclidean distance $\|\mathbf{z}_1 - \mathbf{z}_2\|^2$ or the negative inner product $-\mathbf{z}_1^T \mathbf{z}_2$. In the following we explain the doubly contrastive components with more details.

Contrastive attraction: The intra-positive contrasts is defined in a form of the conditional probability, where the positive samples compete to gain a larger probability to be moved from the query. Here we adapt to CACR a Bayesian strategy in Zheng and Zhou (2020), which exploits the combination of an energy-based likelihood term and a prior distribution, to quantify the difference between two implicit probability distributions given their empirical samples. Specifically, denoting $d_{t^+}(\cdot, \cdot)$ as a distance metric with temperature $t^+ \in \mathbb{R}^+$, *e.g.*, $d_{t^+}(\mathbf{z}_1, \mathbf{z}_2) = t^+ \|\mathbf{z}_1 - \mathbf{z}_2\|^2$, given a query $\mathbf{x} = \mathcal{T}(\mathbf{x}_0, \epsilon_0)$, we define the conditional probability of moving it to positive samples $\mathbf{x}^+ = \mathcal{T}(\mathbf{x}_0, \epsilon^+)$:

$$\pi_{\theta}^+(\mathbf{x}^+ | \mathbf{x}, \mathbf{x}_0) := \frac{e^{d_{t^+}(f_{\theta}(\mathbf{x}), f_{\theta}(\mathbf{x}^+))} p(\mathbf{x}^+ | \mathbf{x}_0)}{Q^+(\mathbf{x} | \mathbf{x}_0)}, \quad Q^+(\mathbf{x} | \mathbf{x}_0) := \int e^{d_{t^+}(f_{\theta}(\mathbf{x}), f_{\theta}(\mathbf{x}^+))} p(\mathbf{x}^+ | \mathbf{x}_0) d\mathbf{x}^+, \tag{3}$$

where $f_{\theta}(\cdot)$ is an encoder parameterized by θ and $Q^+(\mathbf{x})$ is a normalization term. This construction makes it more likely to pull \mathbf{x} towards a positive sample that is more distant in their latent representation space. With Eqn. (3), the contrastive attraction loss \mathcal{L}_{CA} measures the expected cost of moving a query to its positive samples, as defined in Eqn. (2), which more heavily weighs $c(f_{\theta}(\mathbf{x}), f_{\theta}(\mathbf{x}^+))$ if $f_{\theta}(\mathbf{x})$ and $f_{\theta}(\mathbf{x}^+)$ are further away from each other.

Contrastive repulsion: On the contrary of the contrastive attraction shown in Eqn. (3), we define the conditional probability for moving query \mathbf{x} to a negative sample as

$$\pi_{\theta}^-(\mathbf{x}^- | \mathbf{x}) := \frac{e^{-d_{t^-}(f_{\theta}(\mathbf{x}), f_{\theta}(\mathbf{x}^-))} p(\mathbf{x}^-)}{Q^-(\mathbf{x})}, \quad Q^-(\mathbf{x}) := \int e^{-d_{t^-}(f_{\theta}(\mathbf{x}), f_{\theta}(\mathbf{x}^-))} p(\mathbf{x}^-) d\mathbf{x}^-, \tag{4}$$

where $t^- \in \mathbb{R}^+$ is the temperature. This construction makes it more likely to move query \mathbf{x} to a negative sample that is closer from it in their representation space. With Eqn. (4), the contrastive repulsion loss \mathcal{L}_{CR} measures the expected cost to repel negative samples from the query shown in Eqn. (2), which more heavily weighs $c(f_{\theta}(\mathbf{x}), f_{\theta}(\mathbf{x}^-))$ if $f_{\theta}(\mathbf{x})$ and $f_{\theta}(\mathbf{x}^-)$ are closer to each other.

Choice of $c(\cdot, \cdot)$, $d_{t^+}(\cdot, \cdot)$ and $d_{t^-}(\cdot, \cdot)$. There could be various choices for the point-to-point cost function $c(\cdot, \cdot)$, distance metric $d_{t^+}(\cdot, \cdot)$ in Eqn. (3), and $d_{t^-}(\cdot, \cdot)$ in Eqn. (4). Considering the encoder f_{θ} outputs normalized vectors on the surface of a hypersphere, maximizing the inner product is equivalent to minimizing squared Euclidean distance. Without loss of generality, we define them as

$$c(\mathbf{z}_1, \mathbf{z}_2) = \|\mathbf{z}_1 - \mathbf{z}_2\|_2^2, \quad d_{t^+}(\mathbf{z}_1, \mathbf{z}_2) = t^+ \|\mathbf{z}_1 - \mathbf{z}_2\|_2^2, \quad d_{t^-}(\mathbf{z}_1, \mathbf{z}_2) = t^- \|\mathbf{z}_1 - \mathbf{z}_2\|_2^2,$$

where $t^+, t^- \in \mathbb{R}^+$. There are other choices for $c(\cdot, \cdot)$ and we show the ablation study in Section C.4.

3.2 Mini-batch based stochastic optimization

Under the CACR loss as in Eqn. (2), to make the learning of $f_{\theta}(\cdot)$ amenable to mini-batch stochastic gradient descent (SGD) based optimization, we draw $(\mathbf{x}_i^{\text{data}}, \epsilon_i) \sim p_{\text{data}}(\mathbf{x})p(\epsilon)$ for $i = 1, \dots, M$ and then approximate the distribution of the query using an empirical distribution of M samples as

$$\hat{p}(\mathbf{x}) = \frac{1}{M} \sum_{i=1}^M \delta_{\mathbf{x}_i}, \quad \mathbf{x}_i = \mathcal{T}(\mathbf{x}_i^{\text{data}}, \epsilon_i).$$

With query \mathbf{x}_i and $\epsilon_{1:K} \stackrel{iid}{\sim} p(\epsilon)$, we approximate $p(\mathbf{x}_i^-)$ for Eqn. (4) and $p(\mathbf{x}_i^+ | \mathbf{x}_i^{\text{data}})$ for Eqn. (3) as

$$\hat{p}(\mathbf{x}_i^-) = \frac{1}{M-1} \sum_{j \neq i} \delta_{\mathbf{x}_j}, \quad \hat{p}(\mathbf{x}_i^+ | \mathbf{x}_i^{\text{data}}) = \frac{1}{K} \sum_{k=1}^K \delta_{\mathbf{x}_{ik}^+}, \quad \mathbf{x}_{ik}^+ = \mathcal{T}(\mathbf{x}_i^{\text{data}}, \epsilon_k). \tag{5}$$

Note we may improve the accuracy of $\hat{p}(\mathbf{x}_i^-)$ in Eqn. (5) by adding previous queries into the support of this empirical distribution. Other more sophisticated ways to construct negative samples (Oord et al., 2018; He et al., 2020; Khosla et al., 2020) could also be adopted to define $\hat{p}(\mathbf{x}_i^-)$. We will elaborate these points when describing experiments.

Plugging Eqn. (5) into Eqn. (3) and Eqn. (4), we can approximate the conditional distributions as

$$\begin{aligned}\hat{\pi}_{\theta}^{+}(\mathbf{x}_i^{+} | \mathbf{x}_i, \mathbf{x}_i^{\text{data}}) &:= \sum_{k=1}^K \frac{e^{d_{t+}(\mathbf{f}_{\theta}(\mathbf{x}_i), \mathbf{f}_{\theta}(\mathbf{x}_{ik}^{+}))}}{\sum_{k'=1}^K e^{d_{t+}(\mathbf{f}_{\theta}(\mathbf{x}_i), \mathbf{f}_{\theta}(\mathbf{x}_{ik'}^{+}))}} \delta_{\mathbf{x}_{ik}^{+}}, \\ \hat{\pi}_{\theta}^{-}(\mathbf{x}_i^{-} | \mathbf{x}_i) &:= \sum_{j \neq i} \frac{e^{-d_{t-}(\mathbf{f}_{\theta}(\mathbf{x}_i), \mathbf{f}_{\theta}(\mathbf{x}_j))}}{\sum_{j' \neq i} e^{-d_{t-}(\mathbf{f}_{\theta}(\mathbf{x}_i), \mathbf{f}_{\theta}(\mathbf{x}_{j'}))}} \delta_{\mathbf{x}_j},\end{aligned}$$

which leads to a mini-batch based CACR loss as $\hat{\mathcal{L}}_{\text{CACR}} = \hat{\mathcal{L}}_{\text{CA}} + \hat{\mathcal{L}}_{\text{CR}}$, where

$$\begin{aligned}\hat{\mathcal{L}}_{\text{CA}} &:= \frac{1}{M} \sum_{i=1}^M \sum_{k=1}^K \frac{e^{d_{t+}(\mathbf{f}_{\theta}(\mathbf{x}_i), \mathbf{f}_{\theta}(\mathbf{x}_{ik}^{+}))}}{\sum_{k'=1}^K e^{d_{t+}(\mathbf{f}_{\theta}(\mathbf{x}_i), \mathbf{f}_{\theta}(\mathbf{x}_{ik'}^{+}))}} \times c(\mathbf{f}_{\theta}(\mathbf{x}_i), \mathbf{f}_{\theta}(\mathbf{x}_{ik}^{+})), \\ \hat{\mathcal{L}}_{\text{CR}} &:= -\frac{1}{M} \sum_{i=1}^M \sum_{j \neq i} \frac{e^{-d_{t-}(\mathbf{f}_{\theta}(\mathbf{x}_i), \mathbf{f}_{\theta}(\mathbf{x}_j))}}{\sum_{j' \neq i} e^{-d_{t-}(\mathbf{f}_{\theta}(\mathbf{x}_i), \mathbf{f}_{\theta}(\mathbf{x}_{j'}))}} \times c(\mathbf{f}_{\theta}(\mathbf{x}_i), \mathbf{f}_{\theta}(\mathbf{x}_j)).\end{aligned}$$

We optimize θ via SGD using $\nabla_{\theta} \hat{\mathcal{L}}_{\text{CACR}}$, with the framework instantiated as in Figure 2.

Relation with CL: As shown in Eqn. (2), with both the contrastive attraction component and contrastive repulsion component, CACR loss shares the same intuition of conventional CL in pulling positive samples closer to and pushing negative samples away from the query in their representation space. However, CACR realizes this intuition by introducing the double-contrast strategy on the point-to-point moving cost, where the contrasts appear in the intra-comparison within positive and negative samples, respectively. The use of the double-contrast strategy clearly differs the CACR loss in Eqn. (2) from the conventional CL loss in Eqn. (1), which typically relies on a softmax-based contrast formed with a single positive sample and multiple equally-weighted independent negative samples. A summary of the comparison between some representative CL losses and CACR is shown in Table 1.

Table 1: Comparison with representative CL methods. K and M denotes the number of positive and negative samples, respectively.

Method	Contrast Loss	Intra-positive contrast	Intra-negative contrast
CL (Oord et al., 2018)	1-vs- M cross-entropy	✗	✗
AU-CL (Wang and Isola, 2020)	1-vs- M cross-entropy	✗	✗
HN-CL (Robinson et al., 2021)	1-vs- M cross-entropy	✗	✓
CMC (Tian et al., 2019)	$\binom{K}{2} \times (1\text{-vs-}M \text{ cross-entropy})$	✗	✗
CACR (ours)	Intra- K -positive vs Intra- M -negative	✓	✓

4 Property analysis of CACR

4.1 On the contrastive attraction

We first analyze the effects *w.r.t.* the positive samples. With contrastive attraction, the property below suggests that the optimal encoder produces representations invariant to the noisy details.

Property 1. *The contrastive attraction loss \mathcal{L}_{CA} is optimized if and only if all positive samples of a query share the same representation as that query. More specifically, for query \mathbf{x} that is transformed from $\mathbf{x}_0 \sim p_{\text{data}}(\mathbf{x})$, its positive samples share the same representation with it, which means*

$$\mathbf{f}_{\theta}(\mathbf{x}^{+}) = \mathbf{f}_{\theta}(\mathbf{x}) \text{ for any } \mathbf{x}^{+} \sim \pi(\mathbf{x}^{+} | \mathbf{x}, \mathbf{x}_0). \quad (6)$$

This property coincides with the characteristic (learning invariant representation) of the CL loss in Wang and Isola (2020) when achieving the optima. However, the optimization dynamic in contrastive attraction evolves in the context of $\mathbf{x}^{+} \sim \pi_{\theta}(\mathbf{x}^{+} | \mathbf{x}, \mathbf{x}_0)$, which is different from that in the CL.

Lemma 1. *Let us instantiate $c(\mathbf{f}_{\theta}(\mathbf{x}), \mathbf{f}_{\theta}(\mathbf{x}^{+})) = -\mathbf{f}_{\theta}(\mathbf{x})^{\top} \mathbf{f}_{\theta}(\mathbf{x}^{+})$. Then, the contrastive attraction loss \mathcal{L}_{CA} in Eqn. (2) can be re-written as*

$$\mathbb{E}_{\mathbf{x}_0} \mathbb{E}_{\mathbf{x}, \mathbf{x}^{+} \sim p(\cdot | \mathbf{x}_0)} \left[-\mathbf{f}_{\theta}(\mathbf{x})^{\top} \mathbf{f}_{\theta}(\mathbf{x}^{+}) \frac{\pi_{\theta}^{+}(\mathbf{x}^{+} | \mathbf{x}, \mathbf{x}_0)}{p(\mathbf{x}^{+} | \mathbf{x}_0)} \right],$$

which could further reduce to the alignment loss $\mathbb{E}_{\mathbf{x}_0 \sim p_{\text{data}}(\mathbf{x})} \mathbb{E}_{\mathbf{x}, \mathbf{x}^{+} \sim p(\cdot | \mathbf{x}_0)} [-\mathbf{f}_{\theta}(\mathbf{x})^{\top} \mathbf{f}_{\theta}(\mathbf{x}^{+})]$ in (Wang and Isola, 2020), iff $\pi_{\theta}^{+}(\mathbf{x}^{+} | \mathbf{x}, \mathbf{x}_0) = p(\mathbf{x}^{+} | \mathbf{x}_0)$.

Property 1 and Lemma 1 jointly show contrastive attraction in CACR and the alignment loss in CL reach the same optima, while working in different sampling mechanism. In practice \mathbf{x}^{+} and \mathbf{x} are usually independently sampled augmentations in a mini-batch, as shown in Section 3.2, which raises a gap between the empirical distribution and the true distribution. Our method makes the alignment more efficient by considering the intra-relation of these positive samples to the query.

4.2 On the contrastive repulsion

Next we analyze the effects *w.r.t.* the contribution of negative samples. Wang and Isola (2020) reveals that a perfect encoder will uniformly distribute samples on a hypersphere under an uniform isometric assumption, *i.e.*, for any uniformly sampled $\mathbf{x}, \mathbf{x}^- \stackrel{iid}{\sim} p(\mathbf{x})$, their latent representations $\mathbf{z} = f_{\theta}(\mathbf{x})$ and $\mathbf{z}^- = f_{\theta}(\mathbf{x}^-)$ also satisfy $p(\mathbf{z}) = p(\mathbf{z}^-)$. We follow their assumption to analyze contrastive repulsion via the following lemma.

Lemma 2. *Without loss of generality, we define the moving cost and metric in the conditional distribution as $c(\mathbf{z}_1, \mathbf{z}_2) = d(\mathbf{z}_1, \mathbf{z}_2) = \|\mathbf{z}_1 - \mathbf{z}_2\|_2^2$. When we are with an uniform prior, namely $p(\mathbf{x}) = p(\mathbf{x}^-)$ for any $\mathbf{x}, \mathbf{x}^- \stackrel{iid}{\sim} p(\mathbf{x})$ and $p(\mathbf{z}) = p(\mathbf{z}^-)$ given their latent representations $\mathbf{z} = f_{\theta}(\mathbf{x})$ and $\mathbf{z}^- = f_{\theta}(\mathbf{x}^-)$, then optimizing θ with \mathcal{L}_{CR} in Eqn. (2) is the same as optimizing θ to minimize the mutual information between \mathbf{x} and \mathbf{x}^- :*

$$I(X; X^-) = \mathbb{E}_{\mathbf{x} \sim p(\mathbf{x})} \mathbb{E}_{\mathbf{x}^- \sim \pi_{\theta}^-(\cdot | \mathbf{x})} \left[\ln \frac{\pi_{\theta}^-(\mathbf{x}^- | \mathbf{x})}{p(\mathbf{x}^-)} \right], \quad (7)$$

and is also the same as optimizing θ to maximize the conditional differential entropy of \mathbf{x}^- given \mathbf{x} :

$$\mathcal{H}(X^- | X) = \mathbb{E}_{\mathbf{x} \sim p(\mathbf{x})} \mathbb{E}_{\mathbf{x}^- \sim \pi_{\theta}^-(\cdot | \mathbf{x})} [-\ln \pi_{\theta}^-(\mathbf{x}^- | \mathbf{x})]. \quad (8)$$

Here the minimizer θ^* of \mathcal{L}_{CR} is also that of $I(X; X^-)$, whose global minimum zero is attained iff X and X^- are independent, and the equivalent maximum of $\mathcal{H}(X^- | X)$ indicates the optimization of \mathcal{L}_{CR} is essentially aimed towards the uniformity of representation about negative samples.

We notice that one way to reach the optimum suggested in the above lemma is optimizing θ by contrastive repulsion until that for any $\mathbf{x} \sim p(\mathbf{x})$, $d(f_{\theta}(\mathbf{x}), f_{\theta}(\mathbf{x}^-))$ is equal for all $\mathbf{x}^- \sim \pi_{\theta}^-(\cdot | \mathbf{x})$. This means for any sampled negative samples, their representations are also uniformly distributed after contrastive repulsion. Interestingly, this is consistent with the uniformity property achieved by CL (Wang and Isola, 2020), which connects contrastive repulsion with CL in the perspective of negative sample effects.

Note that, although the above analysis builds upon the uniform isometric assumption, our method actually does not rely on it. Here, we formalize a more general relation between the contrastive repulsion and the contribution of negative samples in CL without this assumption as follows.

Lemma 3. *As the number of negative samples M goes to infinity, the contribution of the negative samples to the CL loss become the Uniformity Loss in AU-CL (Wang and Isola, 2020), termed as $\mathcal{L}_{\text{uniform}}$ for simplicity. It can be expressed as an upper bound of \mathcal{L}_{CR} by adding the mutual information $I(X; X^-)$ in Eqn. (7):*

$$\underbrace{\mathbb{E}_{\mathbf{x} \sim p(\mathbf{x})} \left[\ln \mathbb{E}_{\mathbf{x}^- \sim p(\mathbf{x}^-)} e^{f_{\theta}(\mathbf{x}^-)^{\top} f_{\theta}(\mathbf{x}) / \tau} \right]}_{\mathcal{L}_{\text{uniform}}} + I(X; X^-) \geq \mathcal{L}_{\text{CR}},$$

As shown in Lemma 3, the mutual information $I(X; X^-)$ helps quantify the difference between $\mathcal{L}_{\text{uniform}}$ and \mathcal{L}_{CR} . The difference between drawing $\mathbf{x}^- \sim \pi_{\theta}^-(\mathbf{x}^- | \mathbf{x})$ (in CR) and drawing \mathbf{x}^- independently in a mini-batch (in CL) is non-trivial as long as $I(X; X^-)$ is non-zero. In practice, this is true almost everywhere since we have to handle the skewed data distribution in real-world applications, *e.g.*, the label-shift scenarios (Garg et al., 2020). In this view, CR does not require the representation space to be uniform like CL does, and is more robust to the complex cases through considering the intra-contrastive relation within negative samples.

5 Experiments and analysis

We compare the performance of CACR loss with representative CL methods, divided into two different categories according to their positive sampling size: $K = 1$ and $K = 4$. For methods with a single positive sample ($K = 1$), the baseline methods include the conventional CL loss (Oord et al., 2018; Logeswaran and Lee, 2018; Chen et al., 2020d; He et al., 2020), AlignUniform CL loss (AU-CL) (Wang and Isola, 2020), and the non-debiased version of the CL loss with hard negative sampling (HN-CL) (Robinson et al., 2021). In the case of $K = 4$, we take contrastive multi-view coding (CMC) loss (Tian et al., 2019) (align with our augmentation settings and use augmentation views instead of channels) as the comparison baseline. For a fair comparison, on each dataset, we keep for all methods the same experiment setting including learning-rate, mini-batch size, and training epochs, but use their best temperature parameters. Please refer to Appendix B for other detailed experiment setups.

We conduct experiments on five image datasets of varying sizes, including CIFAR-10, CIFAR-100 (Hinton, 2007), and STL-10 (Coates et al., 2011) that are small-scale ones and ImageNet-100 and ImageNet-1K (Deng et al., 2009) that are large-scale ones. Note that ImageNet-100 is a subset of ImageNet-1K, where 100 classes are randomly selected from the standard ImageNet-1K dataset and here we keep the same classes as commonly used in CL works (Tian et al., 2019; Wang and Isola, 2020). For small-scale datasets, we follow SimCLR to construct negative samples as the views augmented from different images within a batch. Moreover, we create two class-imbalanced CIFAR datasets as empirical verification of our theoretical analysis. For large-scale datasets, we follow MoCo-v2 (Chen et al., 2020b) to maintain a queue of negative samples, updated with the momentum-based mechanism. To evaluate the learned representations, following the widely used linear classification protocol, the pre-trained encoder is fixed as a proxy and a linear classifier is added on the top of the base feature encoder for classification. Here we report the Top-1 validation accuracy on these datasets. We also report the results of object detection/segmentation following the transfer learning protocol. The reported numbers for baselines are from the original papers if available, otherwise we report the best ones fine-tuned with the settings according to their corresponding papers.

5.1 Linear classification on small-scale datasets

Classification accuracy: For small-scale datasets, we apply all methods with an AlexNet-based encoder following the setting in Wang and Isola (2020), trained in 200 epochs and with a ResNet50 encoder following the setting in Robinson et al. (2021). The results with the AlexNet-based encoder and ResNet50-based one are summarized in Table 2 and Table 7 (Appendix), respectively. We can observe that in the case of $K = 1$, where the intra-positive contrast of CACR degenerates, CACR slightly outperforms all CL methods. With ResNet50, CACR outperforms with larger margin. Moreover, when $K = 4$, it is interesting to observe an obvious boost in performance, where CMC improves CL by around 2-3% while CACR improves CL by around 3-4%. This supports our analysis that CA is helpful when the intra-positive contrast is not degenerated.

On the effect of CA and CR: To understand the efficacy of the contrasts within positive and negative samples, we illustrate in Figure 3 (Left) the evolution of conditional entropy $\mathcal{H}(X^-|X)$ and classification accuracy *w.r.t.* the training epoch. In each epoch, we calculate the conditional entropy with Eqn. (8) on every mini-batch of size $M = 512$ and take the average across mini-batches. As shown in Figure 3, $\mathcal{H}(X^-|X)$ is getting maximized as the encoder is getting optimized. As shown in Lemma 2, under the uniform data prior assumption, the optimization of CL and CACR encourages the encoder to maximize $\mathcal{H}(X^-|X)$. It is also interesting to observe that in the case with multiple positive samples, the gap between CACR and CMC is much larger in terms of the conditional entropy. This implies the CA module can further boost the repulsion of negative samples. Although CMC uses multiple positive in CL loss, the lack of intra-positive contrast shows the gap of repulsion efficiency. As shown in Figure 3 (Right), CACR consistently outperforms the other methods in linear classification with the learned representations at the same epoch, indicating a superior learning efficiency of CACR. See Appendix C for similar observations On CIFAR-10 and CIFAR-100.

As a qualitative verification, we randomly take a query from a mini-batch, and illustrate its positive and negative samples and their conditional probabilities in Figure 4. As shown, given this query of a dog image, the positive sample with the largest weight contains partial dog information, indicating the encoder to focus on texture information; the negatives with larger weights are more related to the dog category, which encourages the encoder to focus on distinguishing these “hard” negative samples. In total, the weights learned by CACR enjoy the interpretability compared to the conventional CL.

5.2 Linear classification on class-imbalanced datasets

To verify the robustness of CACR in comparison with that of CL when this uniform prior assumption is violated, we create two class-imbalanced datasets with CIFAR-10 and CIFAR-100. Such datasets are created by randomly sampling a certain number of samples from each class with a “linear” or “exponential” rule by following the setting in (Kim et al., 2020). Specifically, given a dataset with C classes, for class $l \in \{1, 2, \dots, C\}$, we randomly take samples with proportion $\lfloor \frac{l}{C} \rfloor$ for “linear” rule and proportion $\exp(\lfloor \frac{l}{C} \rfloor)$ for “exponential” rule. Once the dataset is sampled, it is fixed during training. For evaluation we keep the standard validation/testing datasets. Thus there is a label-shift between training and testing data distribution.

Summarized in Table 3 are the results on class-imbalanced datasets, which show all the methods have a performance drop compared to the results in Table 2. It is clear that CACR has the least performance decline in most cases. Especially, when $K = 4$, CACR shows better performance robustness due to the characteristic of doubly contrastive within positive and negative samples. For

Table 2: The top-1 classification accuracy (%) of different contrastive objectives under the SimCLR framework on small-scale datasets. All methods follow the SimCLR setting and apply an AlexNet-based encoder. The results of CL and AU-CL on STL-10 are quoted from Wang and Isola (2020).

Methods	CIFAR-10	CIFAR-100	STL-10
CL	83.47	55.41	83.89
AU-CL	83.39	55.31	84.43
HN-CL	83.67	55.87	83.27
CACR ($K = 1$)	83.73	56.52	84.51
CMC ($K = 4$)	85.54	58.64	84.50
CACR ($K = 4$)	86.54	59.41	85.59

Table 3: The classification accuracy (%) of different contrastive objectives on class-imbalanced datasets. “Linear” and “Exponential” indicate the number of samples in each class are chosen by following a linear rule or an exponential rule, respectively. The performance drops compared with the performance in Table 2 are shown next to each result.

Imbalance	Linear		Exponential	
	CIFAR-10	CIFAR-100	CIFAR-10	CIFAR-100
CL	79.88 _{3.59↓}	52.29 _{3.57↓}	71.74 _{11.73↓}	43.29 _{12.57↓}
AU-CL	80.25 _{3.14↓}	52.74 _{2.57↓}	71.62 _{11.76↓}	44.38 _{10.93↓}
HN-CL	80.51 _{3.15↓}	52.72 _{3.14↓}	72.74 _{10.93↓}	45.13 _{10.73↓}
CACR ($K = 1$)	80.46 _{3.27↓}	54.12 _{2.40↓}	73.02 _{10.71↓}	46.59 _{9.93↓}
CMC ($K = 4$)	82.20 _{3.34↓}	55.38 _{3.26↓}	74.77 _{10.77↓}	48.87 _{9.77↓}
CACR ($K = 4$)	83.62 _{2.92↓}	56.91 _{2.50↓}	75.89 _{10.65↓}	50.17 _{9.24↓}

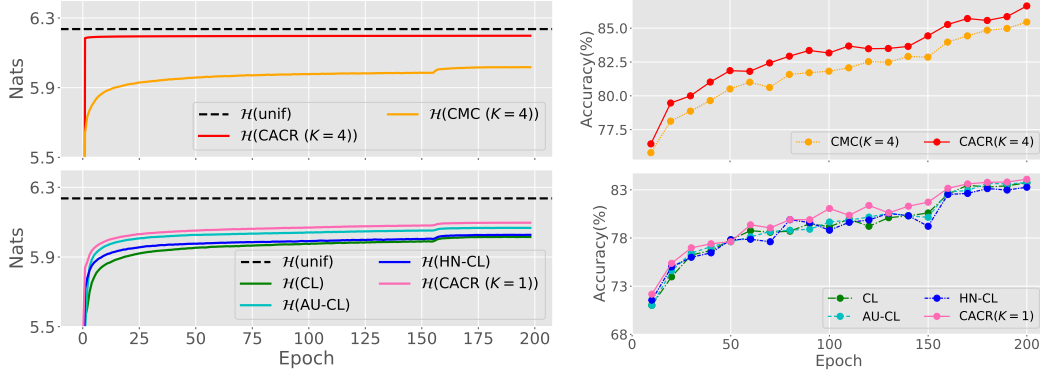


Figure 3: STL-10 training evolution, with mini-batch size 512. **Left:** Conditional entropy $\mathcal{H}(X^-|X)$ *w.r.t.* epoch. The maximal possible conditional entropy is indicated by a dotted line. **Right:** Linear classification with learned representations *w.r.t.* epoch.

example, in the “exponential” setting of CIFAR-100, CL and HN-CL drop 12.57% and 10.73%, respectively, while CACR ($K = 4$) drops 9.24%. It is also interesting to observe HN-CL is relatively better among the baseline methods. According to Robinson et al. (2021), in HN-CL the negative samples are sampled according to the “hardness” *w.r.t.* the query samples with an intra-negative contrast. Its loss could converge to CACR ($K = 1$) with infinite negative samples. This performance gap indicates that directly optimizing the CACR loss could be superior when we have a limited number of samples. With this class-imbalanced datasets, we provide the empirical support to our analysis: When the condition in Lemma 2 is violated, CACR shows a clearer difference than CL and a better robustness with its unique doubly contrastive strategy within positive and negative samples.

5.3 Linear classification on large-scale datasets

For large-scale experiments, following the convention, we adapt all methods into the MoCo-v2 framework and pre-train a ResNet50 encoder in 200 epochs with mini-batch size 128/256 on ImageNet-100/ImageNet-1k. Table 4 summarizes the results of linear classification on these two large-scale datasets. Similar to the case on small-scale datasets, CACR consistently shows better performance, improving the baselines at least by 1.74% on ImageNet-100 and 0.71% on ImageNet-1K. In MoCo-v2, with multiple positive samples, CACR improves the baseline methods by 2.92% on ImageNet-100 and 2.75% on ImageNet-1K. It is worth highlighting that the improvement of CACR is more significant on these large-scale datasets, where the data distribution could be much more diverse compared to these small-scale ones. This is not surprising, as according to our theoretical analysis, CACR’s double-contrast within samples enhances the effectiveness of the encoder’s optimization. Moreover, we can see CACR ($K = 1$) shows a clear improvement over HN-CL. A possible explanation is that although both increasing the negative sample size and selecting hard negatives are proposed to improve the CL loss, the effectiveness of hard negatives is limited when the sampling size is increased over a certain limit. As CACR targets to repel the negative samples away, the conditional distribution still efficiently guides the repulsion when the sampling size becomes large.

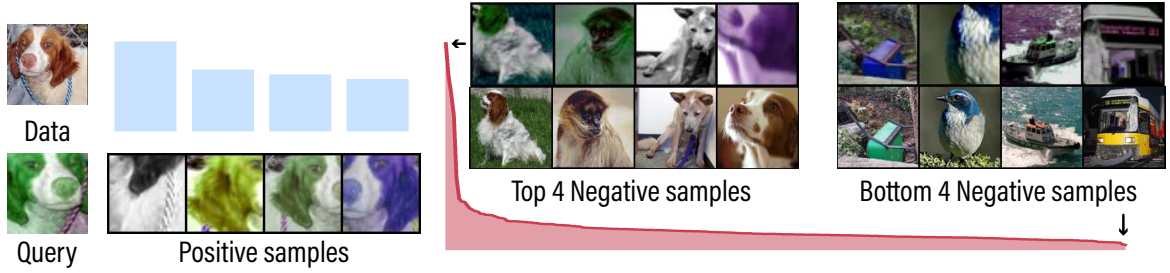


Figure 4: Illustration of positive/negative samples and their corresponding weights. (Left) For a query augmented from the original dog image, 4 positive samples are shown, with their weights visualized as the blue distribution. (Right) The sampling weights of negatives are visualized as the red distribution; we visualize 4 negative samples with the highest and 4 with the lowest weights, with their original images shown below.

Table 4: Top-1 classification accuracy (%) of different objectives with MoCo-v2 framework and ResNet50 encoder on ImageNet dataset. The results from paper or Github page are marked by \star .

Methods	ImageNet-100	ImageNet-1K
CL	77.54 \star	67.50 \star
AU-CL	77.66 \star	67.69 \star
HN-CL	76.34	67.41
CMC ($K = 1$)	75.80 \star	66.20 \star
CACR ($K = 1$)	79.40	68.40
CMC ($K = 4$)	78.84	69.45
CACR ($K = 4$)	80.46	70.35

Table 5: Results of transferring features to object detection and segmentation task on Pascal VOC, with the pre-trained MoCo-v2 ResNet50 on ImageNet-1k. The results of CL loss on Pascal VOC are from their papers and Github pages.

Task	Object Detection						Object Segmentation		
	Pascal VOC			COCO			COCO		
Dataset	AP	AP ₅₀	AP ₇₅	AP	AP ₅₀	AP ₇₅	AP	AP ₅₀	AP ₇₅
Loss	AP	AP ₅₀	AP ₇₅	AP	AP ₅₀	AP ₇₅	AP	AP ₅₀	AP ₇₅
CL	57.00	82.40	63.60	40.90	60.53	44.30	35.73	57.29	38.20
AU-CL	57.24	82.49	63.83	41.01	60.68	44.40	35.56	57.38	37.93
CACR ($K = 1$)	57.75	82.76	64.23	41.08	60.80	44.84	35.74	57.50	38.07
CACR ($K = 4$)	57.91	82.83	64.85	41.50	61.11	45.30	36.08	57.95	38.68

5.4 Object detection and segmentation

A main goal of unsupervised learning is to sufficiently capture general and transferable representations. Besides the linear classification evaluation, we also transfer the pre-trained contrastive models as the initialization for fine-tuning in downstream tasks, such as object detection and segmentation. To evaluate the transfer ability of the learned features, following the protocols in previous works (Tian et al., 2019; He et al., 2020; Chen et al., 2020b; Wang and Isola, 2020), we use the pretrained ResNet50 on ImageNet-1K for object detection and segmentation task on Pascal VOC (Everingham et al., 2010) and COCO (Lin et al., 2014) by using detectron2 (Wu et al., 2019). The experimental setting details are shown in Appendix B.2 and kept the same as He et al. (2020) and Chen et al. (2020b). The test AP, AP₅₀, and AP₇₅ of bounding boxes in object detection and test AP, AP₅₀, and AP₇₅ of masks in segmentation are reported in Table 5. We can observe that the performances of CACR is consistently better than that of other contrastive objectives. For example, compared to CL, the AP has been improved by 0.91% on Pascal VOC object detection and by 0.31% on COCO object segmentation.

6 Conclusion

In this paper, we rethink the limitation of conventional contrastive learning (CL) methods that form the contrastive loss by randomly selecting positive and negative samples for a query. We introduce a novel Contrastive Attraction and Contrastive Repulsion (CACR) loss with a doubly contrastive strategy, which constructs for a random query two contradicting conditional distributions, which model the importance of a positive sample and that of a negative sample, respectively, to the query. To form the contrastive loss, CACR combines the independent and random sampling convention with the practice of contrastively reweighing both positive and negative samples according to their distances to the query. Our theoretical analysis and empirical results show that optimizing the CACR loss can effectively attract positive samples and repel negative ones from the query as CL intends to do, but is more robust in more general cases. Extensive experiments on small, large-scale, and imbalanced datasets consistently demonstrate the superiority and robustness of CACR over the state-of-the-art methods in contrastive representation learning and related downstream tasks.

References

- Aaron van den Oord, Yazhe Li, and Oriol Vinyals. Representation learning with contrastive predictive coding. *arXiv preprint arXiv:1807.03748*, 2018.
- Ben Poole, Sherjil Ozair, Aäron van den Oord, Alexander A Alemi, and George Tucker. On variational lower bounds of mutual information. In *NeurIPS Workshop on Bayesian Deep Learning*, 2018.
- Ishan Misra and Laurens van der Maaten. Self-supervised learning of pretext-invariant representations. In *Proceedings of the IEEE/CVF Conference on Computer Vision and Pattern Recognition*, pages 6707–6717, 2020.
- Kaiming He, Haoqi Fan, Yuxin Wu, Saining Xie, and Ross Girshick. Momentum contrast for unsupervised visual representation learning. In *Proceedings of the IEEE/CVF Conference on Computer Vision and Pattern Recognition (CVPR)*, June 2020.
- Ting Chen, Simon Kornblith, Mohammad Norouzi, and Geoffrey Hinton. A simple framework for contrastive learning of visual representations. *arXiv preprint arXiv:2002.05709*, 2020a.
- Hongchao Fang and Pengtao Xie. CERT: Contrastive self-supervised learning for language understanding. *arXiv preprint arXiv:2005.12766*, 2020.
- John M Giorgi, Osvald Nitski, Gary D. Bader, and Bo Wang. DeCLUTR: Deep contrastive learning for unsupervised textual representations. *ArXiv*, abs/2006.03659, 2020.
- Feng Wang, Xiang Xiang, Jian Cheng, and Alan Loddon Yuille. Normface: L2 hypersphere embedding for face verification. In *Proceedings of the 25th ACM international conference on Multimedia*, pages 1041–1049, 2017.
- Tim R Davidson, Luca Falorsi, Nicola De Cao, Thomas Kipf, and Jakub M Tomczak. Hyperspherical variational auto-encoders. *arXiv preprint arXiv:1804.00891*, 2018.
- R Devon Hjelm, Alex Fedorov, Samuel Lavoie-Marchildon, Karan Grewal, Phil Bachman, Adam Trischler, and Yoshua Bengio. Learning deep representations by mutual information estimation and maximization. In *International Conference on Learning Representations*, 2018.
- Yonglong Tian, Dilip Krishnan, and Phillip Isola. Contrastive multiview coding. *arXiv preprint arXiv:1906.05849*, 2019.
- Philip Bachman, R Devon Hjelm, and William Buchwalter. Learning representations by maximizing mutual information across views. In *Advances in Neural Information Processing Systems*, 2019.
- Tongzhou Wang and Phillip Isola. Understanding contrastive representation learning through alignment and uniformity on the hypersphere. In *International Conference on Machine Learning*, pages 9929–9939. PMLR, 2020.
- Xinlei Chen, Haoqi Fan, Ross Girshick, and Kaiming He. Improved baselines with momentum contrastive learning. *arXiv preprint arXiv:2003.04297*, 2020b.
- Ching-Yao Chuang, Joshua Robinson, Yen-Chen Lin, Antonio Torralba, and Stefanie Jegelka. Debaised contrastive learning. *Advances in Neural Information Processing Systems*, 33, 2020.
- Yannis Kalantidis, Mert Bulent Sariyildiz, Noe Pion, Philippe Weinzaepfel, and Diane Larlus. Hard negative mixing for contrastive learning. *arXiv preprint arXiv:2010.01028*, 2(6), 2020.
- Nikunj Saunshi, Orestis Plevrakis, Sanjeev Arora, Mikhail Khodak, and Hrishikesh Khandeparkar. A theoretical analysis of contrastive unsupervised representation learning. In *International Conference on Machine Learning*, pages 5628–5637. PMLR, 2019.
- Yoshua Bengio, Aaron Courville, and Pascal Vincent. Representation learning: A review and new perspectives. *IEEE transactions on pattern analysis and machine intelligence*, 35(8):1798–1828, 2013.
- Michael E Tipping and Christopher M Bishop. Probabilistic principal component analysis. *Journal of the Royal Statistical Society: Series B (Statistical Methodology)*, 61(3):611–622, 1999.
- Geoffrey E Hinton and Ruslan R Salakhutdinov. Reducing the dimensionality of data with neural networks. *science*, 313(5786):504–507, 2006.

- Diederik P Kingma and Max Welling. Auto-encoding variational Bayes. *International Conference on Learning Representations*, 2014.
- Michael Gutmann and Aapo Hyvärinen. Noise-contrastive estimation: A new estimation principle for unnormalized statistical models. In *Proceedings of the Thirteenth International Conference on Artificial Intelligence and Statistics*, pages 297–304, 2010.
- Michael Tschannen, Josip Djolonga, Paul K Rubenstein, Sylvain Gelly, and Mario Lucic. On mutual information maximization for representation learning. *arXiv preprint arXiv:1907.13625*, 2019.
- Yonglong Tian, Dilip Krishnan, and Phillip Isola. Contrastive representation distillation. In *International Conference on Learning Representations*, 2020a.
- Ting Chen, Simon Kornblith, Kevin Swersky, Mohammad Norouzi, and Geoffrey Hinton. Big self-supervised models are strong semi-supervised learners. *arXiv preprint arXiv:2006.10029*, 2020c.
- Zhirong Wu, Yuanjun Xiong, X Yu Stella, and Dahua Lin. Unsupervised feature learning via non-parametric instance discrimination. In *Proceedings of the IEEE Conference on Computer Vision and Pattern Recognition*, 2018.
- Lajanugen Logeswaran and Honglak Lee. An efficient framework for learning sentence representations. In *International Conference on Learning Representations*, 2018.
- Olivier J Hénaff, Ali Razavi, Carl Doersch, SM Eslami, and Aaron van den Oord. Data-efficient image recognition with contrastive predictive coding. *arXiv preprint arXiv:1905.09272*, 2019.
- Fan-Yun Sun, Jordan Hoffmann, Vikas Verma, and Jian Tang. InfoGraph: Unsupervised and semi-supervised graph-level representation learning via mutual information maximization. In *International Conference on Learning Representations*, 2020.
- Yujia Li, Chenjie Gu, Thomas Dullien, Oriol Vinyals, and Pushmeet Kohli. Graph matching networks for learning the similarity of graph structured objects. In *International Conference on Machine Learning*, pages 3835–3845, 2019.
- Kaveh Hassani and Amir Hosein Khasahmadi. Contrastive multi-view representation learning on graphs. In *International Conference on Machine Learning*, pages 3451–3461, 2020.
- Petar Velickovic, William Fedus, William L Hamilton, Pietro Liò, Yoshua Bengio, and R Devon Hjelm. Deep Graph Infomax. In *International Conference on Learning Representations*, 2019.
- Aravind Srinivas, Michael Laskin, and Pieter Abbeel. CURL: Contrastive unsupervised representations for reinforcement learning. In *International Conference on Machine Learning*, pages 10360–10371, 2020.
- Prannay Khosla, Piotr Teterwak, Chen Wang, Aaron Sarna, Yonglong Tian, Phillip Isola, Aaron Maschinot, Ce Liu, and Dilip Krishnan. Supervised contrastive learning. *Advances in Neural Information Processing Systems*, 33, 2020.
- Tristan Sylvain, Linda Petrini, and Devon Hjelm. Locality and compositionality in zero-shot learning. In *International Conference on Learning Representations*, 2020.
- Yonglong Tian, Chen Sun, Ben Poole, Dilip Krishnan, Cordelia Schmid, and Phillip Isola. What makes for good views for contrastive learning. In *Advances in Neural Information Processing Systems*, 2020b.
- Avishek Joey Bose, Huan Ling, and Yanshuai Cao. Adversarial contrastive estimation. *arXiv preprint arXiv:1805.03642*, 2018.
- Anoop Cherian and Shuchin Aeron. Representation learning via adversarially-contrastive optimal transport. *arXiv preprint arXiv:2007.05840*, 2020.
- Chunyuan Li, Xiujun Li, Lei Zhang, Baolin Peng, Mingyuan Zhou, and Jianfeng Gao. Self-supervised pre-training with hard examples improves visual representations. *arXiv preprint arXiv:2012.13493*, 2020.
- Mike Wu, Milan Mosse, Chengxu Zhuang, Daniel Yamins, and Noah Goodman. Conditional negative sampling for contrastive learning of visual representations. In *International Conference on Learning Representations*, 2021.

- Joshua David Robinson, Ching-Yao Chuang, Suvrit Sra, and Stefanie Jegelka. Contrastive learning with hard negative samples. In *International Conference on Learning Representations*, 2021.
- Huangjie Zheng and Mingyuan Zhou. Comparing probability distributions with conditional transport. *arXiv preprint arXiv:2012.14100*, 2020.
- Saurabh Garg, Yifan Wu, Sivaraman Balakrishnan, and Zachary C Lipton. A unified view of label shift estimation. *arXiv preprint arXiv:2003.07554*, 2020.
- Xu Chen, Ya Zhang, Ivor Tsang, and Yuangang Pan. Learning robust node representations on graphs. *arXiv preprint arXiv:2008.11416*, 2020d.
- Geoffrey E Hinton. Learning multiple layers of representation. *Trends in cognitive sciences*, 11(10): 428–434, 2007.
- Adam Coates, Andrew Ng, and Honglak Lee. An analysis of single-layer networks in unsupervised feature learning. In *Proceedings of the fourteenth international conference on artificial intelligence and statistics*, pages 215–223, 2011.
- Jia Deng, Wei Dong, Richard Socher, Li-Jia Li, Kai Li, and Li Fei-Fei. Imagenet: A large-scale hierarchical image database. In *2009 IEEE conference on computer vision and pattern recognition*, pages 248–255. Ieee, 2009.
- Yechan Kim, Younkwan Lee, and Moongu Jeon. Imbalanced image classification with complement cross entropy. *arXiv preprint arXiv:2009.02189*, 2020.
- Mark Everingham, Luc Van Gool, Christopher KI Williams, John Winn, and Andrew Zisserman. The pascal visual object classes (VOC) challenge. *International journal of computer vision*, 88(2): 303–338, 2010.
- Tsung-Yi Lin, Michael Maire, Serge Belongie, James Hays, Pietro Perona, Deva Ramanan, Piotr Dollár, and C Lawrence Zitnick. Microsoft COCO: Common objects in context. In *European conference on computer vision*, pages 740–755. Springer, 2014.
- Yuxin Wu, Alexander Kirillov, Francisco Massa, Wan-Yen Lo, and Ross Girshick. Detectron2. <https://github.com/facebookresearch/detectron2>, 2019.
- Priya Goyal, Piotr Dollár, Ross Girshick, Pieter Noordhuis, Lukasz Wesolowski, Aapo Kyrola, Andrew Tulloch, Yangqing Jia, and Kaiming He. Accurate, large minibatch SGD: Training imagenet in 1 hour. *arXiv preprint arXiv:1706.02677*, 2017.
- K. He, X. Zhang, S. Ren, and J. Sun. Deep residual learning for image recognition. In *2016 IEEE Conference on Computer Vision and Pattern Recognition (CVPR)*, pages 770–778, 2016. doi: 10.1109/CVPR.2016.90.
- Shaoqing Ren, Kaiming He, Ross Girshick, and Jian Sun. Faster R-CNN: towards real-time object detection with region proposal networks. *IEEE transactions on pattern analysis and machine intelligence*, 39(6):1137–1149, 2016.
- Kaiming He, Georgia Gkioxari, Piotr Dollár, and Ross Girshick. Mask R-CNN. In *Proceedings of the IEEE international conference on computer vision*, pages 2961–2969, 2017.
- Laurens van der Maaten and Geoffrey Hinton. Visualizing data using t-SNE. *Journal of Machine Learning Research*, 9(86):2579–2605, 2008.

Contrastive Attraction and Contrastive Repulsion for Representation Learning: Appendix

A Proofs and detailed derivation

Proof of Property 1. By definition, the point-to-point cost $c(\mathbf{z}_1, \mathbf{z}_2)$ is always non-negative. Without loss of generality, we define it with the Euclidean distance. When Eqn. (6) is true, the expected cost of moving between a pair of positive samples, as defined as \mathcal{L}_{CA} in Eqn. (2), will reach its minimum at 0. When Eqn. (6) is not true, by definition we will have $\mathcal{L}_{CA} > 0$, i.e., $\mathcal{L}_{CA} = 0$ is possible only if Eqn. (6) is true. \square

Proof of Lemma 1. By changing the reference distribution of the expectation from $\pi_{\theta}^+(\cdot | \mathbf{x}, \mathbf{x}_0)$ to $p(\cdot | \mathbf{x}_0)$, we can directly re-write the CA loss as:

$$\begin{aligned}\mathcal{L}_{CA} &= \mathbb{E}_{\mathbf{x} \sim p(\mathbf{x})} \mathbb{E}_{\mathbf{x}^+ \sim \pi_{\theta}^+(\cdot | \mathbf{x}, \mathbf{x}_0)} [c(f_{\theta}(\mathbf{x}), f_{\theta}(\mathbf{x}^+))] \\ &= \mathbb{E}_{\mathbf{x}_0} \mathbb{E}_{\mathbf{x}, \mathbf{x}^+ \sim p(\cdot | \mathbf{x}_0)} \left[-f_{\theta}(\mathbf{x})^{\top} f_{\theta}(\mathbf{x}^+) \frac{\pi_{\theta}^+(\mathbf{x}^+ | \mathbf{x}, \mathbf{x}_0)}{p(\mathbf{x}^+ | \mathbf{x}_0)} \right],\end{aligned}$$

which complete the proof. \square

Proof of Lemma 2. Denoting

$$Z(\mathbf{x}) = \int e^{-d(f_{\theta}(\mathbf{x}), f_{\theta}(\mathbf{x}^-))} p(\mathbf{x}^-) d\mathbf{x}^-,$$

we have

$$\ln \pi_{\theta}^-(\mathbf{x}^- | \mathbf{x}) = -d(f_{\theta}(\mathbf{x}), f_{\theta}(\mathbf{x}^-)) + \ln p(\mathbf{x}^-) - \ln Z(\mathbf{x}).$$

Thus we have

$$\begin{aligned}\mathcal{L}_{CR} &= \mathbb{E}_{\mathbf{x} \sim p(\mathbf{x})} \mathbb{E}_{\mathbf{x}^- \sim \pi_{\theta}^-(\cdot | \mathbf{x})} [\ln \pi_{\theta}^-(\mathbf{x}^- | \mathbf{x}) - \ln p(\mathbf{x}^-) + \ln Z(\mathbf{x})] \\ &= C_1 + C_2 - \mathcal{H}(X^- | X)\end{aligned}\tag{9}$$

where $C_1 = \mathbb{E}_{\mathbf{x} \sim p(\mathbf{x})} \mathbb{E}_{\mathbf{x}^- \sim \pi_{\theta}^-(\cdot | \mathbf{x})} [\ln p(\mathbf{x}^-)]$ and $C_2 = -\mathbb{E}_{\mathbf{x} \sim p(\mathbf{x})} \ln Z(\mathbf{x})$. Under the assumption of a uniform prior on $p(\mathbf{x})$, C_1 becomes a term that is not related to θ . Under the assumption of a uniform prior on $p(\mathbf{z})$, where $\mathbf{z} = f_{\theta}(\mathbf{x})$, we have

$$\begin{aligned}Z(\mathbf{x}) &= \mathbb{E}_{\mathbf{x}^- \sim p(\mathbf{x})} [e^{-d(f_{\theta}(\mathbf{x}), f_{\theta}(\mathbf{x}^-))}] \\ &= \mathbb{E}_{\mathbf{z}^- \sim p(\mathbf{z})} [e^{-(\mathbf{z}^- - \mathbf{z})^{\top} (\mathbf{z}^- - \mathbf{z})}] \\ &\propto \int e^{-(\mathbf{z}^- - \mathbf{z})^{\top} (\mathbf{z}^- - \mathbf{z})} d\mathbf{z}^- \\ &= \sqrt{\pi},\end{aligned}\tag{10}$$

which is also not related to θ . Therefore, under the uniform prior assumption on both $p(\mathbf{x})$ and $p(\mathbf{z})$, minimizing \mathcal{L}_{CR} is the same as maximizing $\mathcal{H}(X^- | X)$, as well as the same as minimizing $I(X, X^-)$. \square

Proof of Lemma 3. The CL loss can be decomposed as an expected dissimilarity term and a log-sum-exp term:

$$\begin{aligned}\mathcal{L}_{CL} &:= \mathbb{E}_{(\mathbf{x}, \mathbf{x}^+, \mathbf{x}_{1:M}^-)} \left[-\ln \frac{e^{f_{\theta}(\mathbf{x})^{\top} f_{\theta}(\mathbf{x}^+)/\tau}}{e^{f_{\theta}(\mathbf{x})^{\top} f_{\theta}(\mathbf{x}^+)/\tau} + \sum_i e^{f_{\theta}(\mathbf{x}_i^-)^{\top} f_{\theta}(\mathbf{x})/\tau}} \right] \\ &= \mathbb{E}_{(\mathbf{x}, \mathbf{x}^+)} \left[-\frac{1}{\tau} f_{\theta}(\mathbf{x})^{\top} f_{\theta}(\mathbf{x}^+) \right] + \mathbb{E}_{(\mathbf{x}, \mathbf{x}^+, \mathbf{x}_{1:M}^-)} \left[\ln \left(e^{f_{\theta}(\mathbf{x})^{\top} f_{\theta}(\mathbf{x}^+)/\tau} + \sum_{i=1}^M e^{f_{\theta}(\mathbf{x}_i^-)^{\top} f_{\theta}(\mathbf{x})/\tau} \right) \right],\end{aligned}$$

where the positive sample \mathbf{x}^+ is independent of \mathbf{x} given \mathbf{x}_0 and the negative samples \mathbf{x}_i^- are independent of \mathbf{x} . As the number of negative samples goes to infinity, following Wang and Isola (2020), the normalized CL loss is decomposed into the sum of the align loss, which describes the contribution of the positive samples, and the uniform loss, which describes the contribution of the negative samples:

$$\lim_{M \rightarrow \infty} \mathcal{L}_{CL} - \ln M = \underbrace{\mathbb{E}_{(\mathbf{x}, \mathbf{x}^+)} \left[-\frac{1}{\tau} f_{\theta}(\mathbf{x})^{\top} f_{\theta}(\mathbf{x}^+) \right]}_{\text{contribution of positive samples}} + \underbrace{\mathbb{E}_{\mathbf{x} \sim p(\mathbf{x})} \left[\ln \mathbb{E}_{\mathbf{x}^- \sim p(\mathbf{x}^-)} e^{f_{\theta}(\mathbf{x}^-)^{\top} f_{\theta}(\mathbf{x})/\tau} \right]}_{\text{contribution of negative samples}}$$

With importance sampling, the second term in the RHS of the above equation can be further derived into:

$$\begin{aligned} & \mathbb{E}_{\mathbf{x} \sim p(\mathbf{x})} \left[\ln \mathbb{E}_{\mathbf{x}^- \sim p(\mathbf{x}^-)} e^{f_{\boldsymbol{\theta}}(\mathbf{x}^-)^\top f_{\boldsymbol{\theta}}(\mathbf{x})/\tau} \right] \\ &= \mathbb{E}_{\mathbf{x} \sim p(\mathbf{x})} \left[\ln \mathbb{E}_{\mathbf{x}^- \sim \pi_{\boldsymbol{\theta}}(\mathbf{x}^- | \mathbf{x})} \left[e^{f_{\boldsymbol{\theta}}(\mathbf{x}^-)^\top f_{\boldsymbol{\theta}}(\mathbf{x})/\tau} \frac{p(\mathbf{x}^-)}{\pi_{\boldsymbol{\theta}}(\mathbf{x}^- | \mathbf{x})} \right] \right] \end{aligned}$$

Apply the Jensen inequality, the second term is decomposed into the negative cost plus a log density ratio:

$$\begin{aligned} & \mathbb{E}_{\mathbf{x} \sim p(\mathbf{x})} \left[\ln \mathbb{E}_{\mathbf{x}^- \sim p(\mathbf{x}^-)} e^{f_{\boldsymbol{\theta}}(\mathbf{x}^-)^\top f_{\boldsymbol{\theta}}(\mathbf{x})/\tau} \right] \\ & \geq \mathbb{E}_{\mathbf{x} \sim p(\mathbf{x})} \left[\mathbb{E}_{\mathbf{x}^- \sim \pi_{\boldsymbol{\theta}}(\mathbf{x}^- | \mathbf{x})} [f_{\boldsymbol{\theta}}(\mathbf{x}^-)^\top f_{\boldsymbol{\theta}}(\mathbf{x})/\tau] \right] + \mathbb{E}_{\mathbf{x} \sim p(\mathbf{x})} \left[\mathbb{E}_{\mathbf{x}^- \sim \pi_{\boldsymbol{\theta}}(\mathbf{x}^- | \mathbf{x})} \left[\ln \frac{p(\mathbf{x}^-)}{\pi_{\boldsymbol{\theta}}(\mathbf{x}^- | \mathbf{x})} \right] \right] \\ &= \mathbb{E}_{\mathbf{x} \sim p(\mathbf{x})} \left[\mathbb{E}_{\mathbf{x}^- \sim \pi_{\boldsymbol{\theta}}(\mathbf{x}^- | \mathbf{x})} [f_{\boldsymbol{\theta}}(\mathbf{x}^-)^\top f_{\boldsymbol{\theta}}(\mathbf{x})/\tau] \right] - I(X; X^-) \end{aligned}$$

Defining the point-to-point cost function between two unit-norm vectors as $c(\mathbf{z}_1, \mathbf{z}_2) = -\mathbf{z}_1^\top \mathbf{z}_2$ (same as the Euclidean cost since $\|\mathbf{z}_1 - \mathbf{z}_2\|_2^2/2 = 1 - \mathbf{z}_1^\top \mathbf{z}_2$), we have

$$\begin{aligned} & \mathbb{E}_{\mathbf{x} \sim p(\mathbf{x})} \left[\ln \mathbb{E}_{\mathbf{x}^- \sim p(\mathbf{x}^-)} e^{f_{\boldsymbol{\theta}}(\mathbf{x}^-)^\top f_{\boldsymbol{\theta}}(\mathbf{x})/\tau} \right] + I(X; X^-) \\ & \geq \mathbb{E}_{\mathbf{x} \sim p(\mathbf{x})} \left[\mathbb{E}_{\mathbf{x}^- \sim \pi_{\boldsymbol{\theta}}(\mathbf{x}^- | \mathbf{x})} [f_{\boldsymbol{\theta}}(\mathbf{x}^-)^\top f_{\boldsymbol{\theta}}(\mathbf{x})/\tau] \right] \\ &= - \mathbb{E}_{\mathbf{x} \sim p(\mathbf{x})} \left[\mathbb{E}_{\mathbf{x}^- \sim \pi_{\boldsymbol{\theta}}(\mathbf{x}^- | \mathbf{x})} [c(f_{\boldsymbol{\theta}}(\mathbf{x}^-), f_{\boldsymbol{\theta}}(\mathbf{x}))/\tau] \right] \\ &= \mathcal{L}_{\text{CR}}. \end{aligned}$$

This concludes the relation between the contribution of the negative samples in CL and that in CACR. \square

B Experiment details

On small-scale datasets, all experiments are conducted on a single GPU, including NVIDIA 1080 Ti and RTX 3090; on large-scale datasets, all experiments are done on 8 Tesla-V100-32G GPUs.

B.1 Small-scale datasets: CIFAR-10, CIFAR-100, and STL-10

For experiments on CIFAR-10, CIFAR-100, and STL-10, we use the following configurations:

- **Data Augmentation:** We strictly follow the standard data augmentations to construct positive and negative samples introduced in prior works in contrastive learning (Wu et al., 2018; Tian et al., 2019; Hjelm et al., 2018; Bachman et al., 2019; Chuang et al., 2020; He et al., 2020; Wang and Isola, 2020). The augmentations include image resizing, random cropping, flipping, color jittering, and gray-scale conversion. We provide a Pytorch-style augmentation code in Algorithm 1, which is exactly the same as the one used in Wang and Isola (2020).

Algorithm 1 PyTorch-like Augmentation Code on CIFAR-10, CIFAR-100 and STL-10

```
import torchvision.transforms as transforms

# CIFAR-10 Transformation
def transform_cifar10():
    return transforms.Compose([
        transforms.RandomResizedCrop(32, scale=(0.2, 1)),
        transforms.RandomHorizontalFlip(), # by default p=0.5
        transforms.ColorJitter(0.4, 0.4, 0.4, 0.4),
        transforms.RandomGrayscale(p=0.2),
        transforms.ToTensor(), # normalize to value in [0,1]
        transforms.Normalize(
            (0.4914, 0.4822, 0.4465),
            (0.2023, 0.1994, 0.2010),
        )
    ])

# CIFAR-100 Transformation
def transform_cifar100():
    return transforms.Compose([
        transforms.RandomResizedCrop(32, scale=(0.2, 1)),
        transforms.RandomHorizontalFlip(), # by default p=0.5
        transforms.ColorJitter(0.4, 0.4, 0.4, 0.4),
        transforms.RandomGrayscale(p=0.2),
        transforms.ToTensor(), # normalize to value in [0,1]
        transforms.Normalize(
            (0.5071, 0.4867, 0.4408),
            (0.2675, 0.2565, 0.2761),
        )
    ])

# STL-10 Transformation
def transform_stl10():
    return transforms.Compose([
        transforms.RandomResizedCrop(64, scale=(0.08, 1)),
        transforms.RandomHorizontalFlip(), # by default p=0.5
        transforms.ColorJitter(0.4, 0.4, 0.4, 0.4),
        transforms.RandomGrayscale(p=0.2),
        transforms.ToTensor(), # normalize to value in [0,1]
        transforms.Normalize(
            (0.4409, 0.4279, 0.3868),
            (0.2683, 0.2610, 0.2687),
        )
    ])

])
```

- **Feature Encoder:** Following the experiments in Wang and Isola (2020), we use an AlexNet-based encoder as the feature encoder for these three datasets, where encoder architectures are the same as those used in the corresponding experiments in Tian et al. (2019) and Wang and Isola (2020). Moreover, we also follow the setups in Robinson et al. (2021) and test the performance of CACR with a ResNet50 encoder (results are shown in Table 7).
- **Model Optimization:** We apply the mini-batch SGD with 0.9 momentum and 1e-4 weight decay. The learning rate is linearly scaled as 0.12 per 256 batch size (Goyal et al., 2017). The optimization is done over 200 epochs, and the learning rate is decayed by a factor of 0.1 at epoch 155, 170, and 185.

Table 6: The 100 randomly selected classes from ImageNet forms the ImageNet-100 dataset. These classes are the same as (Wang and Isola, 2020; Tian et al., 2019).

ImageNet-100 Classes									
n02869837	n01749939	n02488291	n02107142	n13037406	n02091831	n04517823	n04589890	n03062245	n01773797
n01735189	n07831146	n07753275	n03085013	n04485082	n02105505	n01983481	n02788148	n03530642	n04435653
n02086910	n02859443	n13040303	n03594734	n02085620	n02099849	n01558993	n04493381	n02109047	n04111531
n02877765	n04429376	n02009229	n01978455	n02106550	n01820546	n01692333	n07714571	n02974003	n02114855
n03785016	n03764736	n03775546	n02087046	n07836838	n04099969	n04592741	n03891251	n02701002	n03379051
n02259212	n07715103	n03947888	n04026417	n02326432	n03637318	n01980166	n02113799	n02086240	n03903868
n02483362	n04127249	n02089973	n03017168	n02093428	n02804414	n02396427	n04418357	n02172182	n01729322
n02113978	n03787032	n02089867	n02119022	n03777754	n04238763	n02231487	n03032252	n02138441	n02104029
n03837869	n03494278	n04136333	n03794056	n03492542	n02018207	n04067472	n03930630	n03584829	n02123045
n04229816	n02100583	n03642806	n04336792	n03259280	n02116738	n02108089	n03424325	n01855672	n02090622

- **Parameter Setup:** On CIFAR-10, CIFAR-100, and STL-10, we follow Wang and Isola (2020) to set the training batch size as $M = 768$ for baselines. The hyper-parameters of CL, AU-CL¹, and HN-CL² are set according to the original paper or online codes. Specifically, the temperature parameter of CL is $\tau = 0.19$, the hyper-parameters of AU-CL are $t = 2.0, \tau = 0.19$, and the hyper-parameter of HN-CL are $\tau = 0.5, \beta = 1.0$ ³, which shows the best performance according to our tuning. For CMC and CACR with multiple positives, the positive sampling size is $K = 4$. To make sure the performance is not improved by using more samples, the training batch size is set as $M = 128$. For CACR, in both single and multi-positive sample settings, we set $t^+ = 1.0$ for all small-scale datasets. As for t^- , for CACR ($K = 1$), t^- is 2.0, 3.0, and 3.0 on CIFAR-10, CIFAR100, and STL-10, respectively. For CACR ($K = 4$), t^- is 0.9, 2.0, and 2.0 on CIFAR-10, CIFAR100, and STL-10, respectively. For further ablation studies, we test t^+ and t^- with the search in the range of $[0.5, 0.7, 0.9, 1.0, 2.0, 3.0]$, and we test all the methods with several mini-batch sizes $M \in \{64, 128, 256, 512, 768\}$.
- **Evaluation:** The feature encoder is trained with the default built-in training set of the datasets. In the evaluation, the feature encoder is frozen, and a linear classifier is trained and tested on the default training set and validation set of each dataset, respectively. Following Wang and Isola (2020), we train the linear classifier with Adam optimizer over 100 epochs, with $\beta_1 = 0.5$, $\beta_2 = 0.999$, $\epsilon = 10^{-8}$, and 128 as the batch size. The initial learning rate is 0.001 and decayed by a factor of 0.2 at epoch 60 and epoch 80. Extracted features from “fc7” are employed for the evaluation. For the ResNet50 setting in Robinson et al. (2021), the extracted features are from the encoder backbone with dimension 2048.

B.2 Large-scale datasets: ImageNet-100 and ImageNet-1K

For large-scale datasets, the Imagenet-1K is the standard ImageNet dataset that has about 1.28 million images of 1000 classes. The ImageNet-100 contains randomly selected 100 classes from the standard ImageNet-1K dataset, and the classes used here are the same with Tian et al. (2019) and Wang and Isola (2020), listed in Table 6. We follow the standard settings in these works and describe the experiment configurations as follows:

- **Data Augmentation:** Following Tian et al. (2019; 2020b); Wang and Isola (2020); Chuang et al. (2020); He et al. (2020), and Chen et al. (2020b), the data augmentations are the same as the standard protocol, including resizing, 1x image cropping, horizontal flipping, color jittering, and gray-scale conversion with specific probability. The full augmentation combination is shown in Algorithm 2.
- **Feature Encoder:** On these two datasets, we apply the MoCo-v2 framework (Chen et al., 2020b), where the ResNet50 (He et al., 2016) is a commonly chosen feature encoder architecture. The output dimension of the encoder is set as 128.
- **Model Optimization:** Following the standard setting in He et al. (2020); Chen et al. (2020b); Wang and Isola (2020), the training mini-batch size is set as 128 on ImageNet-100 and 256 on ImageNet-1K. We use a mini-batch stochastic gradient descent (SGD) optimizer with 0.9 momentum and $1e-4$ weight decay. The total number of training epochs is set as 200. The

¹https://github.com/SsnL/align_uniform

²<https://github.com/joshr17/HCL>

³Please refer to the original paper for the specific meanings of the hyper-parameter in baselines.

Algorithm 2 PyTorch-like Augmentation Code on ImageNet-100 and ImageNet-1K

```
import torchvision.transforms as transforms
# ImageNet-100 and ImageNet-1K Transformation
# MoCo v2's aug: similar to SimCLR https://arxiv.org/abs/2002.05709
def transform_imagenet():
    return transforms.Compose([
        transforms.RandomResizedCrop(224, scale=(0.2, 1.)),
        transforms.RandomApply([transforms.ColorJitter(0.4, 0.4, 0.4, 0.1)
                                ], p=0.8),
        transforms.RandomGrayscale(p=0.2),
        transforms.RandomApply([moco.loader.GaussianBlur([.1, 2.])], p=0.5),
        transforms.RandomHorizontalFlip(),
        transforms.ToTensor(),
        transforms.Normalize(mean=[0.485, 0.456, 0.406],
                             std=[0.229, 0.224, 0.225])
    ])
```

learning rate is initialized as 0.03, decayed by a cosine scheduler for MoCo-V2 at epoch 120 and epoch 160. In all experiments, the momentum of updating the offline encoder is 0.999.

- **Parameter Setup:** On ImageNet-100 and ImageNet-1K, for all methods, the queue size for negative sampling is 65,536. The training batch size is 128 on ImageNet-100 and 256 on ImageNet. For CACR, we train with two positive sampling sizes $K = 1$ and $K = 4$ and the parameters in the conditional weight metric are respectively set as $t^+ = 1.0$, $t^- = 2.0$. For baselines, according to their papers and Github pages (Tian et al., 2019; Wang and Isola, 2020; Robinson et al., 2021), the temperature parameter of CL is $\tau = 0.2$, the hyper-parameters of AU-CL are $t = 3.0$, $\tau = 0.2$, and the hyper-parameters of HN-CL are $\tau = 0.5$, $\beta = 1.0$. Note that CMC ($K = 1$) reported in the main paper is trained with 240 epochs and with its own augmentation methods (Tian et al., 2019). For CMC ($K = 4$), the temperature is set $\tau = 0.07$ according to the setting in Tian et al. (2019) and the loss is calculated with Equation (8) in the paper, which requires more GPU resources than 8 Tesla-V100-32G GPUs with the setting on ImageNet-1K.
- **Linear Classification Evaluation:** Following the standard linear classification evaluation (He et al., 2020; Chen et al., 2020b; Wang and Isola, 2020), the pre-trained feature encoders are fixed, and a linear classifier added on top is trained on the train split and test on the validation split. The linear classifier is trained with SGD over 100 epochs, with the momentum as 0.9, the mini-batch size as 256, and the learning rate as 30.0, decayed by a factor of 0.1 at epoch 60 and epoch 80.
- **Feature Transferring Evaluation (Detection and Segmentation):** The pre-trained models are transferred to various tasks including PASCAL VOC⁴ and COCO⁵ datasets. Strictly following the same setting in He et al. (2020), for the detection on Pascal VOC, a Faster R-CNN (Ren et al., 2016) with an R50-C4 backbone is first fine-tuned end-to-end on the VOC 07+12 trainval set and then evaluated on the VOC 07 test set with the COCO suite of metrics (Lin et al., 2014). The image scale is [480, 800] pixels during training and 800 at inference. For the detection and segmentation on COCO dataset, a Mask R-CNN (He et al., 2017) with C4 backbone (1x schedule) is applied for the end-to-end fine-tuning. The model is tuned on the train2017 set and evaluate on val2017 set, where the image scale is in [640, 800] pixels during training and is 800 in the inference.
- **Estimation of $\hat{\pi}_{\theta}^-$ with MoCo-v2:** Following the strategy in Wang and Isola (2020), we estimate $\hat{\pi}_{\theta}^-$ with not only the cost between queries and keys, but also with the cost between queries. Specifically, at each iteration, let M be the mini-batch size, N be the queue size, $\{f_{q_i}\}_{i=1}^M$ be the query features, and $\{f_{k_j}\}_{j=1}^N$ be the key features. The conditional distribution is calculated as:

$$\hat{\pi}_{\theta}^-(\cdot|f_{q_i}) = \frac{e^{-d_{t^-}(\cdot, f_{q_i})}}{\sum_{j=1}^N e^{-d_{t^-}(f_{k_j}, f_{q_i})} + \sum_{j \neq i} e^{-d_{t^-}(f_{q_j}, f_{q_i})}}$$

To be clear, the Pytorch-like pseudo-code is provided in Algorithm 3. In MoCo-v2 framework, as the keys are produced from the momentum encoder, this estimation could help the main encoder get involved with the gradient from the conditional distribution, which is consistent with the formulation in Section 3.2.

⁴<http://host.robots.ox.ac.uk/pascal/VOC/index.html>

⁵<https://cocodataset.org/#download>

Algorithm 3 PyTorch-like style pseudo-code of CACR with MoCo-v2 at each iteration.

```
##### Inputs #####
# t_pos, t_neg: hyper-parameters in CACR
# m: momentum
# im_list=[B0, B2, ..., BK] list of mini-batches of length (K+1)
# B: mini-batches (Mx3x224x224), M denotes batch_size
# encoder_q: main encoder; encoder_k: momentum encoder
# queue: dictionary as a queue of N features of keys (dxN); d denotes the feature dimension

##### compute the embeddings of all samples #####
q_list = [encoder_q(im) for im in im_list] # a list of (K+1) queries q: M x d
k_list = [encoder_k(im) for im in im_list]
stacked_k = torch.stack(k_list, dim=0) # keys k: (K+1) x M x d

##### compute the loss #####
CACR_loss_pos, CACR_loss_neg = 0.0, 0.0
for k in range(len(im_list)): #load a mini-batch with M samples as queries
    q = q_list[k]
    mask = list(range(len(im_list)))
    mask.pop(k) # the rest mini-batches are used as positive and negative samples

    ##### compute the positive cost #####
    # calculate the cost of moving positive samples: M x K
    cost_for_pos = (q - stacked_k[mask]).norm(p=2, dim=-1).pow(2).transpose(1, 0) # point-to-point cost
    with torch.no_grad(): # the calculation involves momentum encoder, so with no grad here.
        # calculate the conditional distribution: M x K
        weights_for_pos = torch.softmax(cost_for_pos.mul(t_pos), dim=1) # calculate the positive conditional
        distribution
    # calculate the positive cost with the empirical mean
    CACR_loss_pos += (cost_for_pos*weights_for_pos).sum(1).mean()

    ##### compute the loss of negative samples #####
    # calculate the cost and weights of negative samples from the queue: M x K
    sq_dists_for_cost = (2 - 2 * mm(q, queue))
    sq_dists_for_weights = sq_dists_for_cost

    if with_intra_batch: # compute the distance of negative samples in the mini-batch: Mx(M-1)
        intra_batch_sq_dists = torch.norm(q[:,None] - q, dim=-1).pow(2).masked_select(~torch.eye(q.shape[0], dtype=
            bool).cuda()).view(q.shape[0], q.shape[0] - 1)
        # combine the distance of negative samples from the queue and intra-batch: Mx(K+M-1)
        sq_dists_for_cost = torch.cat([sq_dists_for_cost, intra_batch_sq_dists], dim=1)
        sq_dists_for_weights = torch.cat([sq_dists_for_weights, intra_batch_sq_dists], dim=1)

    # calculate the negative conditional distribution: if with_intra_batch==True Mx(K+M-1), else MxK
    weights_for_neg = torch.softmax(sq_dists_for_weights.mul(-t_neg), dim=1)
    # calculate the negative cost with the empirical mean
    CACR_loss_neg += (sq_dists_for_cost.mul(-1.0)*weights_for_neg).sum(1).mean()

# combine the loss of positive cost and negative cost and update main encoder
CACR_loss = CACR_loss_pos/len(im_list)+CACR_loss_neg/len(im_list)
CACR_loss.backward()
update(encoder_q.params) # SGD update: main encoder
encoder_k.params = m*encoder_k.params+(1-m)*encoder_q.params #momentum update: key encoder

# update the dictionary, dequeue and enqueue
enqueue(queue, k_list[-1]) # enqueue the current minibatch
dequeue(queue) # dequeue the earliest minibatch
```

pow: power function; mm: matrix multiplication; cat: concatenation.

C Additional experimental results

In this section, we provide additional results in our experiments, including ablation studies, and corresponding qualitative results.

C.1 Results with ResNet50 on small-scale datasets

As an additional results on small-scale datasets, we test the performance of CACR with ResNet50 as a different encoder backbone. Here we strictly follow the same setting of Robinson et al. (2021), and the results are shown in Table 7. We can observe with ResNet50 encoder backbone, CACR with single positive or multiple positive pairs consistently outperform the baselines. Compared with the results in Table 2, the CACR shows a more clear improvement over the CL baselines.

Table 7: The top-1 classification accuracy (%) of different contrastive objectives with SimCLR framework on small-scale datasets. All methods follow SimCLR setting and apply a ResNet50 encoder and trained with 400 epochs.

Dataset	CL	AU-CL	HN-CL	CACR(K=1)	CMC(K=4)	CACR(K=4)
CIFAR-10	88.70	88.63	89.02	90.97	90.05	92.89
CIFAR-100	62.00	62.57	62.96	62.98	65.19	66.52
STL-10	84.60	83.81	84.29	88.42	91.40	93.04

C.2 On the effects of conditional distribution

Uniform Attraction and Uniform Repulsion: A degenerated version of CACR

To reinforce the necessity of the contrasts within positives and negatives before the attraction and repulsion, we introduce a degenerated version of CACR here, where the conditional distributions are forced to be uniform. Remind $c(\mathbf{z}_1, \mathbf{z}_2)$ as the point-to-point cost of moving between two vectors \mathbf{z}_1 and \mathbf{z}_2 , *e.g.*, the squared Euclidean distance $\|\mathbf{z}_1 - \mathbf{z}_2\|^2$ or the negative inner product $-\mathbf{z}_1^T \mathbf{z}_2$. In the same spirit of (1), we have considered a uniform attraction and uniform repulsion (UAUR) without doubly contrasts within positive and negative samples, whose objective is

$$\min_{\theta} \left\{ \mathbb{E}_{\mathbf{x}_0 \sim p_{data}(\mathbf{x})} \mathbb{E}_{\epsilon_0, \epsilon^+ \sim p(\epsilon)} [c(f_{\theta}(\mathbf{x}), f_{\theta}(\mathbf{x}^+))] - \mathbb{E}_{\mathbf{x}, \mathbf{x}^- \sim p(\mathbf{x})} [c(f_{\theta}(\mathbf{x}), f_{\theta}(\mathbf{x}^-))] \right\}. \quad (11)$$

The intuition of UAUR is to minimize/maximize the expected cost of moving the representations of positive/negative samples to that of the query, with the costs of all sample pairs being uniformly weighted. While Eqn. (1) has been proven to be effective for representation learning, our experimental results do not find Eqn. (11) to perform well, suggesting that the success of representation learning is not guaranteed by uniformly pulling positive samples towards and pushing negative samples away from the query.

Distinction between CACR and UAUR: Compared to UAUR in Eqn. (11) that uniformly weighs different pairs, CACR is distinct in considering the dependency between samples: as the latent-space distance between the query and its positive sample becomes larger, the conditional probability becomes higher, encouraging the encoder to focus more on the alignment of this pair. In the opposite, as the distance between the query and its negative sample becomes smaller, the conditional probability becomes higher, encouraging the encoder to push them away from each other.

In order to further explore the effects of the conditional distribution, we conduct an ablation study to compare the performance of different variants of CACR with/without conditional distributions. Here, we compare 4 configurations of CACR ($K = 4$): (i) CACR with both positive and negative conditional distribution; (ii) CACR without the positive conditional distribution; (iii) CACR without the negative conditional distribution; (iv) CACR without both positive and negative conditional distributions, which refers to UAUR model (see Equation 11). As shown in Table 8, when discarding the positive conditional distribution, the linear classification accuracy slightly drops. As the negative conditional distribution is discarded, there is a large performance drop compared to the full CACR objective. With the modeling of neither positive nor negative conditional distribution, the UAUR shows a continuous performance drop, suggesting that the success of representation learning is not guaranteed by uniformly pulling positive samples closer and pushing negative samples away. The comparison between these CACR variants shows the necessity of the conditional distribution.

Supplementary studies of CA and CR: As a continuous ablation study shown in Figure 3, we also conduct similar experiments on CIFAR-100 and STL-10, where we study the evolution of conditional entropy $\mathcal{H}(X^-|X)$ and classification accuracy *w.r.t.* the training epoch. Remind in each epoch, we calculate the conditional entropy with Eqn. (8) on every mini-batch of size $M = 512$ (the

Table 8: Linear classification performance (%) of different variants of our method. “CACR” represents the normal CACR configuration, “w/o π_{θ}^+ ” means without the positive conditional distribution, “w/o π_{θ}^- ” means without the negative conditional distribution. “UAUR” indicates the uniform cost (see the model we discussed in Equation 11), *i.e.* without both positive and negative conditional distribution. This experiment is done on all small-scale datasets, with $K = 4$ and mini-batch size $M = 128$.

Methods	CIFAR-10	CIFAR-100	STL-10
CACR	85.94	59.51	85.59
w/o π_{θ}^+	85.22	58.74	85.06
w/o π_{θ}^-	78.49	47.88	72.94
UAUR	77.17	44.24	71.88

Table 9: The top-1 classification accuracy (%) of different contrastive objectives with different training epochs on small-scale datasets, following SimCLR setting and applying the AlexNet-based encoder.

Dataset	Trained with 400 epochs				Trained with 200 epochs	
	CL	AU-CL	HN-CL	CACR(K=1)	CMC(K=4)	CACR(K=4)
CIFAR-10	83.61	83.57	83.72	83.86	85.54	86.54
CIFAR-100	55.41	56.07	55.80	56.41	58.64	59.41
STL-10	83.49	83.43	82.41	84.56	84.50	85.59

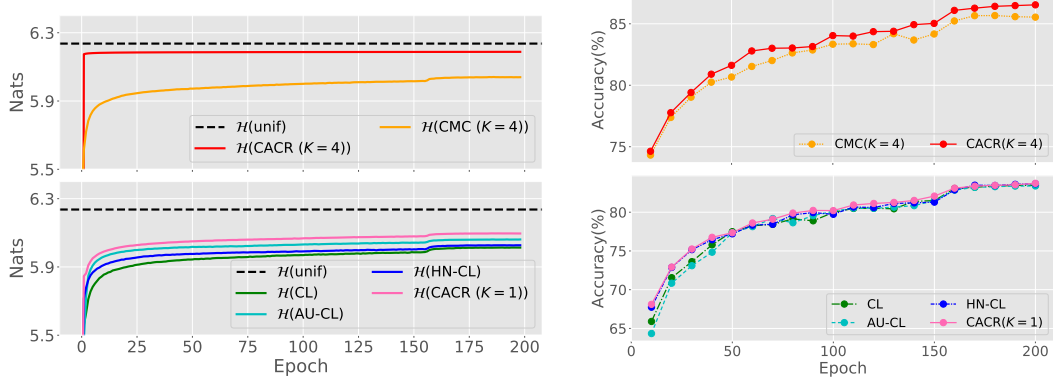
last mini-batch will be ignored if the size is not 512) and take the average across the mini-batches. The results are shown in Figure 5. Similar to the observation on CIFAR-10, shown in Figure 3, we can observe $\mathcal{H}(X^-|X)$ is getting maximized as the encoder is getting optimized with these methods, which confirms Lemma 2. On the right panels, the linear classification results with learned representations is plotted every 10 epochs. We can observe CACR consistently provides better performance than the other methods at the same epoch, indicating the efficiency of CACR.

As qualitative illustrations, we randomly fix one mini-batch, and randomly select one sample as the query. Then we extract the features with the encoder trained with CL loss and CACR ($K = 1$) loss at epochs 1, 20, and 200, and visualize the (four) positives and negatives in the embedding space with t -SNE (van der Maaten and Hinton, 2008). For more clear illustration, we center the query in the middle of the plot and only show samples appearing in the range of $[-10, 10]$ on both x and y axis. The results are shown in Figure 6(c), from which we can find that as the encoder is getting trained, the positive samples are aligned closer and the negative samples are pushed away for both methods. Compared to the encoder trained with CL, we can observe CACR shows better performance in achieving this goal. Moreover, we can observe the distance between any two data points in the plot is more uniform, which confirms that CACR shows better results in the maximization of the conditional entropy $\mathcal{H}(X^-|X)$.

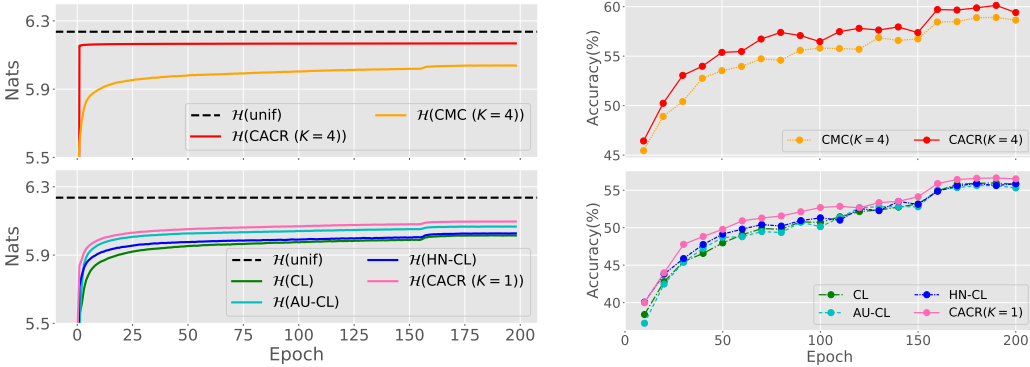
C.3 Ablation study

Does CACR($K \geq 2$) outperform by seeing more samples? To address this concern, in our main paper, we intentionally decrease the mini-batch size as $M = 128$. Thus the total number of samples used per iteration is not greater than those used when $K = 1$. To further justify if the performance boost comes from seeing more samples when using multiple positive pairs, we also let the methods allowing single positive pair train with double epochs. As shown in Table 9, we can observe even trained with 400 epochs, the performance of methods using single positive pair still have a gap from those using multiple positive pairs.

On the effects of sampling size: We investigate the model performance and robustness with different sampling size by varying the mini-batch size used in the training. On all the small-scale datasets, the mini-batches are applied with size 64, 128, 256, 512, 768 and the corresponding linear classification results are shown in Figure 7. From this figure, we can see that CACR ($K = 4$) consistently achieves better performance than other objectives. For example, when mini-batch size is 256, CACR ($K = 4$) outperforms CMC by about 0.4%-1.2%. CACR ($K = 1$) shows better performance in most of the cases, while slightly underperforms than the baselines with mini-batch size 64. A possible explanation could be the estimation of the conditional distribution needs more samples to provide good guidance for the encoder.



(a) Entropy and classification accuracy *w.r.t.* epoch (CIFAR-10)



(b) Entropy and classification accuracy *w.r.t.* epoch (CIFAR-100)

Figure 5: (*Supplementary to Figure 3*) Training evolution on CIFAR-10 and CIFAR-100, with mini-batch size 512. **Left:** Conditional entropy $\mathcal{H}(X^-|X)$ *w.r.t.* training epoch. The maximal possible conditional entropy is indicated by a dotted line. **Right:** Linear classification with learned representations *w.r.t.* training epoch.

On the effects of hyper-parameter t^+ , t^- : Remind in the definition of positive and negative conditional distribution, two hyper-parameters t^+ and t^- are involved as following:

$$\pi_{\theta}^+(\mathbf{x}^+|\mathbf{x}, \mathbf{x}_0) := \frac{e^{t^+ \|f_{\theta}(\mathbf{x}) - f_{\theta}(\mathbf{x}^+)\|^2} p(\mathbf{x}^+|\mathbf{x}_0)}{\int e^{t^+ \|f_{\theta}(\mathbf{x}) - f_{\theta}(\mathbf{x}^+)\|^2} p(\mathbf{x}^+|\mathbf{x}_0) d\mathbf{x}^+}; \quad \pi_{\theta}^-(\mathbf{x}^-|\mathbf{x}) := \frac{e^{-t^- \|f_{\theta}(\mathbf{x}) - f_{\theta}(\mathbf{x}^-)\|^2} p(\mathbf{x}^-)}{\int e^{-t^- \|f_{\theta}(\mathbf{x}) - f_{\theta}(\mathbf{x}^-)\|^2} p(\mathbf{x}^-) d\mathbf{x}^-}.$$

In this part, we investigate the effects of t^+ and t^- on representation learning performance on small-scale datasets, with mini-batch size 768 ($K=1$) and 128 ($K=4$) as an ablation study. We search in a range $\{0.5, 0.7, 0.9, 1.0, 2.0, 3.0\}$. The results are shown in Table 10 and Table 11.

Table 10: The classification accuracy(%) of CACR ($K=4$, $M=128$) with different hyper-parameters t^+ on small-scale datasets.

Method	Dataset	0.5	0.7	0.9	1.0	2.0	3.0
CACR ($K=4$)	CIFAR-10	86.07	85.78	85.90	86.54	84.85	84.76
	CIFAR-100	59.47	59.61	59.41	59.41	57.82	57.55
	STL-10	85.90	85.91	85.81	85.59	85.65	85.14

As shown in these two tables, from Table 10, we observe the CACR shows better performance with smaller values for t^+ . Especially when t^+ increases to 3.0, the performance drops up to about 1.9% on CIFAR-100. For analysis, since we have $K=4$ positive samples for the computation of positive conditional distribution, using a large value for t^+ could result in an over-sparse conditional distribution, where the conditional probability is dominant by one or two positive samples. This also explains why the performance when $t^+=3.0$ is close to the classification accuracy of CACR ($K=1$).

Similarly, from Table 11, we can see that a small value for t^- will lead to the degenerated performance. Here, since we are using mini-batches of size 768 ($K=1$) and 128 ($K=4$), a small value for t^- will flatten the weights of the negative pairs and make the conditional distribution closer to a uniform distribution, which explains why the performance when $t^-=0.5$ is close to those without

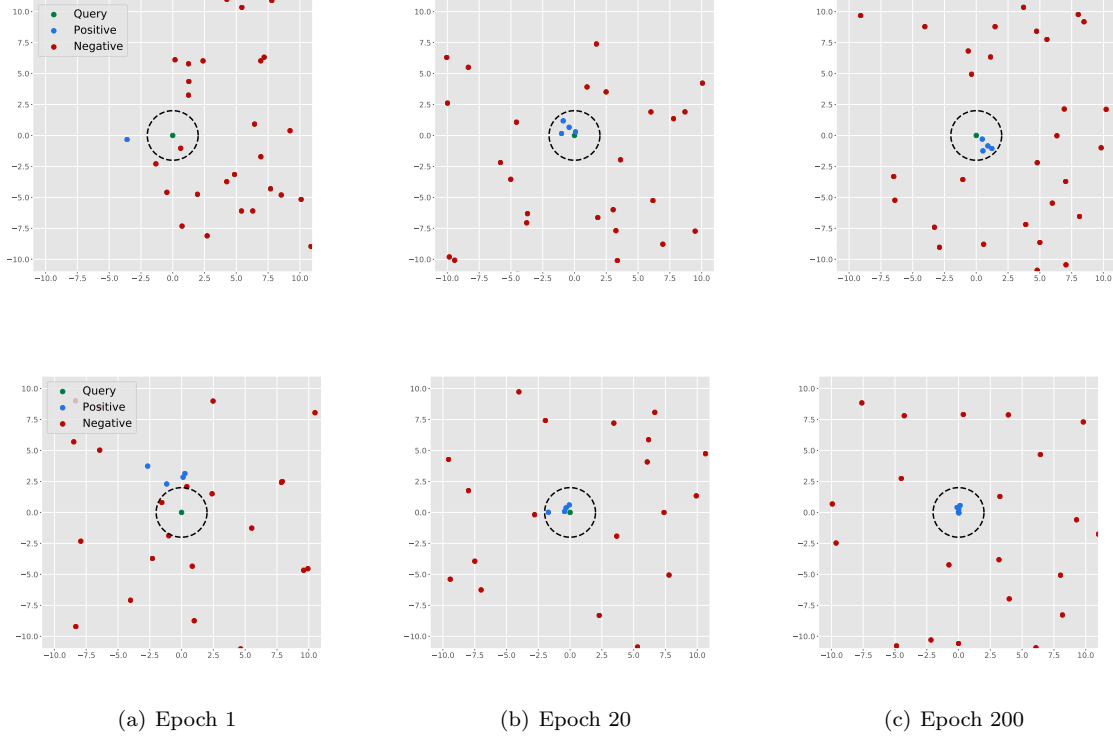


Figure 6: The t -SNE visualization of the latent space at different training epochs, learned by CL loss (*top*) and CACR loss (*bottom*). The picked query is marked in green, with its positive samples marked in blue and its negative samples marked in red. The circle with radius t^- is shown as the black dashed line. As the encoder gets trained, we can observe the positive samples are aligned closer to the query (Property 1), and the conditional differential entropy $\mathcal{H}(X^-|X)$ is progressively maximized, driving the distances $d(f_{\theta}(\mathbf{x}), f_{\theta}(\mathbf{x}^-))$ towards uniform (Lemma 2).

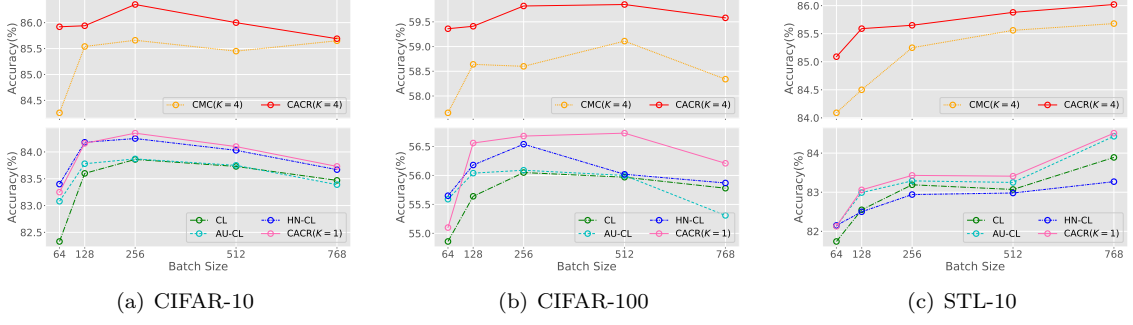


Figure 7: The linear classification results of training with different sampling size on small-scale datasets. The training batch size is proportional to the negative sampling size.

Table 11: The classification accuracy(%) of CACR ($K = 1$, $M = 768$) and CACR ($K = 4$, $M = 128$) with different hyper-parameters t^- on small-scale datasets.

Methods	Dataset	0.5	0.7	0.9	1.0	2.0	3.0
CACR ($K = 1$)	CIFAR-10	81.66	82.40	83.07	82.74	83.73	83.11
	CIFAR-100	51.42	52.81	53.36	54.20	56.21	56.52
	STL-10	80.37	81.47	84.46	82.16	84.21	84.51
CACR ($K = 4$)	CIFAR-10	85.67	86.19	86.54	86.41	85.94	85.69
	CIFAR-100	58.17	58.63	59.37	59.35	59.41	59.31
	STL-10	83.81	84.42	84.71	85.25	85.59	85.41

modeling π_{θ}^- . Based on these results, the values of $t^+ \in [0.5, 1.0]$ and $t^- \in [0.9, 2.0]$ could be good empirical choices according to our experiment settings on these datasets.

C.4 Results of different cost metrics

Recall that the definition of the point-to-point cost metric is usually set as the quadratic Euclidean distance:

$$c(f_{\theta}(\mathbf{x}), f_{\theta}(\mathbf{y})) = \|f_{\theta}(\mathbf{x}) - f_{\theta}(\mathbf{y})\|_2^2. \quad (12)$$

In practice, the cost metric defined in our method is flexible to be any valid metrics. Here, we also investigate the performance when using the Radial Basis Function (RBF) cost metrics:

$$c_{\text{RBF}}(f_{\theta}(\mathbf{x}), f_{\theta}(\mathbf{y})) = -e^{-t\|f_{\theta}(\mathbf{x}) - f_{\theta}(\mathbf{y})\|_2^2}, \quad (13)$$

where $t \in \mathbb{R}^+$ is the precision of the Gaussian kernel. With this definition of the cost metric, our method is closely related to the baseline method AU-CL (Wang and Isola, 2020), where the authors calculate pair-wise RBF cost for the loss *w.r.t.* negative samples. Following Wang and Isola (2020), we replace the cost metric when calculate the negative repulsion cost with the RBF cost and modify $\hat{\mathcal{L}}_{\text{CR}}$ as:

$$\begin{aligned} \hat{\mathcal{L}}_{\text{CR-RBF}} &:= \ln \left[\frac{1}{M} \sum_{i=1}^M \sum_{j \neq i} \frac{e^{-d_{t-}(f_{\theta}(\mathbf{x}_i), f_{\theta}(\mathbf{x}_j))}}{\sum_{j' \neq i} e^{-d_{t-}(f_{\theta}(\mathbf{x}_i), f_{\theta}(\mathbf{x}_{j'}))}} \times c_{\text{RBF}}(f_{\theta}(\mathbf{x}_i), f_{\theta}(\mathbf{x}_j)) \right] \\ &= \ln \left[\frac{1}{M} \sum_{i=1}^M \sum_{j \neq i} \frac{e^{-d_{t-}(f_{\theta}(\mathbf{x}_i), f_{\theta}(\mathbf{x}_j))}}{\sum_{j' \neq i} e^{-d_{t-}(f_{\theta}(\mathbf{x}_i), f_{\theta}(\mathbf{x}_{j'}))}} \times e^{-t\|f_{\theta}(\mathbf{x}_i) - f_{\theta}(\mathbf{x}_j)\|_2^2} \right]. \end{aligned} \quad (14)$$

Here the negative cost is in log scale for numerical stability. When using the RBF cost metric, we use the same setting in the previous experiments and evaluate the linear classification on all small-scale datasets. The results of using Euclidean and RBF cost metrics are shown in Table 12. From this table, we see that both metrics achieve comparable performance, suggesting the RBF cost is also valid in our framework. In CACR, the cost metric measures the cost of different sample pairs and is not limited on specific formulations. More favorable cost metrics can be explored in the future.

Discussion: Relationship with CT. The CT framework of Zheng and Zhou (2020) is primarily focused on measuring the difference between two different distributions, which are referred to as the source and target distributions, respectively. It defines the expected CT cost from the source to target

Table 12: The classification accuracy (%) of CACR ($K = 1$) and CACR ($K = 4$) with different cost metrics on CIFAR-10, CIFAR-100 and STL-10. Euclidean indicates the cost defined in Eqn. 12, and RBF indicates the cost metrics defined in Eqn. 13.

Methods	Cost Metric	CIFAR-10	CIFAR-100	STL-10
CACR($K = 1$)	Euclidean	83.73	56.21	83.55
	RBF	83.08	55.90	84.20
CACR($K = 4$)	Euclidean	85.94	59.41	85.59
	RBF	86.20	58.81	85.80

distributions as the forward CT, and that from the target to source as the backward CT. Minimizing the combined backward and forward CT cost, the primary goal is to optimize the target distribution to approximate the source distribution. By contrast, in CACR, since the marginal distributions of \mathbf{x} and \mathbf{x}^+ are the same and these of \mathbf{x} and \mathbf{x}^- are also the same, there is no need to differentiate the transporting directions. In addition, the primary goal of CACR is not to regenerate the data but to learn $f_{\theta}(\cdot)$ that can provide good latent representations for downstream tasks.